JMC2-FR

1989

LOW TEMPERATURE MÖSSBAUER SPECTROSCOPY OF TIN CATALYSTS

Final Report

by

G. Denes

Work on this project was conducted under the auspices of
Canada Centre for Mineral and Energy Technology,
Energy, Mines and Resources Canada

DSS FILE NUMBER	:	37ST.23440-6-9097
DSS CONTRACT SERIAL NUMBER	:	23440-6-9097/01ST
NRS SCIENTIFIC AUTHORITY	:	Dr. J. MONNIER

MICROMEDIA

CONCORDIA UNIVERSITY
DEPARTMENT OF CHEMISTRY
AND
LABORATORIES FOR INORGANIC MATERIALS
LABORATORY OF SOLID STATE CHEMISTRY AND MÖSSBAUER SPECTROSCOPY
MONTREAL, QUEBEC, CANADA

100 pp

INDEX

List of tables..... 4

List of figures..... 5

Summary..... 7

Résumé..... 9

Introduction..... 12

Theory of the Mössbauer effect and the recoil-free fraction..... 25
1. Recoil energy and thermal broadening..... 25
2. The Mössbauer effect..... 26
3. Effect of temperature and lattice strength on the recoil-free fraction..... 29
3.1. Effect of lattice strength..... 29
3.2. Effect of temperature: recoil-free fraction and Debye-Waller factor..... 31
3.3. Use of variable temperature Mössbauer spectroscopy for quantitative analysis of mixtures..... 35

Experimental..... 38
1. Sample manipulation..... 38
2. Scanning electron microscopy..... 38
3. X-ray powder diffraction..... 38
4. Mössbauer spectroscopy..... 40

Results and discussion..... 49
1. Catalyst supports..... 49
1.1. Hydrous titanate supports and by-products..... 49
1.2. Coal support..... 49
2. Non-calcined catalysts..... 52
2.1. Introduction..... 52
2.2. Tin impregnated coal (JM5)..... 52
2.2.1. X-ray powder diffraction..... 52
2.2.2. Ambient temperature ^{119}Sn Mössbauer spectroscopy..... 52
2.2.3. Variable temperature ^{119}Sn Mössbauer spectroscopy..... 53
2.3. Tin catalysts supported on hydrous titanate..... 56
3. Calcined catalysts..... 60
3.1. Introduction..... 60

3.2. Calcined tin titanate catalysts..... 60
3.3. Calcined cobalt-molybdenum titanate catalysts... 61
3.3.1. Scanning electron microscopy..... 61
3.3.1.1. Sample #64 (JM23): MB-592 (150 °C)..... 62
3.3.1.2. Sample #65 (JM24): MB-592 (350 °C)..... 62
3.3.1.3. Sample #66 (JM25): MB-592 (500 °C)..... 62
3.3.2. X-ray powder diffraction. 71
4. Used catalysts..... 75
4.1. Introduction..... 76
4.2. Tin-119 Mössbauer spectroscopy at ambient temperature.....77
4.3. Tin-119 Mössbauer spectroscopy at low temperature..... 81

Conclusion..... 91

Recommendations..... 97

References..... 98

LIST OF TABLES

I. List of samples studied..... 14

II. Some analytical data for the samples investigated..... 20

III. Techniques used to study the samples..... 23

IV. Energetics of γ_0-ray emission and absorption..... 25

V. Typical energies for nuclear and chemical interactions. 28

VI. Experimental parameters for Mössbauer runs..... 39

VII. Ambient temperature tin-119 Mössbauer isomer shift (relative to $CaSnO_3$) and quadrupole splitting of MB-590 (JM5) coal impregnated with $SnCl_2.2H_2O$, and related compounds..... 53

VIII. Results of the search for mixed oxides of Ti, Co and/or Mo in JM25, using the JCPDS Powder Diffraction File 74

IX. Mössbauer spectroscopic results at ambient temperature for the used catalysts..... 78

X. Estimation of the relative amounts of tin(IV) oxide and SnS in the used catalysts after correction for difference in recoil-free fractions using variable temperature Mössbauer spectroscopy..... 90

LIST OF FIGURES

1. Diagram of samples history..... 16

2. Statistical distribution in the γ-ray energy for (a) emission, (b) absorption, and (c) resonant overlap for successive emission and absorption..... 27

3. Coordination of tin(IV) and tin(II) in inorganic ionic and iono-covalent solids..... 30

4. Evolution of the recoil-free fraction with temperature and as a function of lattice strength..... 34

5. Air Products basic cryogenic system..... 44

6. Air Products vacuum shroud model DMX-20 for low temperature Mössbauer spectroscopy..... 45

7. Set up of the Air Products Displex closed cycle helium refrigerator for low temperature Mössbauer spectroscopy.. 46

8. X-ray powder pattern of the precipitate obtained when Ti(IV) isopropoxide is added to a solution of NaOH (wt 15%) in methanol at RT, after filtration only (JM29) and after washing with ethanol then filtration (JM30).... 50

9. X-ray powder pattern of (a) Coal Forestburg C and (b) the Sn/coal catalyst (JM5)..... 51

10. Evolution of the log of the relative intensity of the tin-119 Mössbauer signal versus temperature for Sn/coal (MB-590, JM5)..... 55

11. Evolution of the log of the relative intensity of the tin(IV) Mössbauer signal in (a) non-calcined catalysts and (b) calcined catalysts..... 59

12. SEM x100 of JM23: MB-592 calcined at 150 °C..... 63

13. (a) SEM x500 of JM23: MB-592 calcined at 150 °C..... 64
(b) SEM x500 of JM23: MB-592 calcined at 150 °C..... 64

14. (a) SEM x2000 of JM23: MB-592 calcined at 150 °C..... 65
(b) SEM x2000 of JM23: MB-592 calcined at 150 °C..... 65
(c) SEM x2000 of JM23: MB-592 calcined at 150 °C..... 66

15. SEM x100 of JM24: MB-592 calcined at 350 °C..... 66

16. (a) SEM x500 of JM24: MB-592 calcined at 350 °C..... 67
(b) SEM x500 of JM24: MB-592 calcined at 350 °C..... 67

17. SEM x2000 of JM24: MB-592 calcined at 350 °C..... 68

18. SEM x100 of JM25: MB-592 calcined at 500 °C..... 68

19. (a) SEM x500 of JM25: MB-592 calcined at 500 °C..... 69
(b) SEM x500 of JM25: MB-592 calcined at 500 °C..... 69

20. (a) SEM x2000 of JM25: MB-592 calcined at 500 °C..... 70
(b) SEM x2000 of JM25: MB-592 calcined at 500 °C..... 70

21. X-ray powder diffraction patterns of MB-592 Co-Mo catalyst deposited on hydrous titanate, after calcination at 150 °C, 350 °C and 500 °C, respectively, and of commercial TiO_2 anatase 72

22. Evolution of the log of the relative intensity of the tin(IV) Mössbauer signal and of SnS in JM4 used catalyst..... 82

23. Ratio SnS/Total tin Mössbauer signal versus temperature for JM4 used catalyst..... 83

24. Relative tin-119 Mössbauer signal versus temperature for JM11 used catalyst..... 84

25. Evolution of the log of the relative intensity of the tin(IV) Mössbauer signal and of SnS in JM11 used catalyst..... 85

26. Ratio SnS/Total tin Mössbauer signal versus temperature for JM11 used catalyst..... 86

27. Relative tin-119 Mössbauer signal versus temperature for JM12 used catalyst..... 87

28. Ratio SnS/Total tin Mössbauer signal versus temperature for JM12 used catalyst..... 88

29. Difference between the % amount of SnS and its % Mössbauer signal in the used catalysts..... 89

30. Comparison of the lattice strength of the stable tin species encountered in tin catalysts supported on hydrous titanate or on coal, as probed by the change of recoil-free fraction versus temperature in tin-119 Mössbauer spectroscopy..... 94

SUMMARY

The purpose of the research presented in this report was to characterize some tin and cobalt-molybdenum containing catalysts supported on a titanium-oxygen framework, improperly called "hydrous titanates". The catalysts were prepared and supplied to us by Dr. Jacques Monnier, Energy Research Laboratories, Canada Centre for Mineral and Energy Technology (CANMET), Energy, Mines and Resources Canada (EMR). A large part of this work was concerned with further studies of samples characterized under an earlier contract [G. Denes, "Characterization of Tin Catalysts by Mössbauer Spectroscopy, Final Report to DSS, SN # 0ST85-00243, 1987]. Tin-119 Mössbauer spectroscopy was used to probe the tin sites in order to determine the tin oxidation state, evaluate the relative abundance of divalent and tetravalent tin, study the tin environment, and identify the tin-containing species. Powder X-ray diffraction showed whether the samples were crystalline, microcrystalline or amorphous, and when Bragg peaks were observed, crystalline phases could be identified and the average particle diameter of microcrystalline phases determined. The texture of the solid catalysts and the particle size and shape were determined by scanning electron microscopy (SEM). It was found that all samples were amorphous or microcrystalline, and calcination resulted in growth of the particles, however, these were found to be usually in the range 100-350 Å after calcination, and well below 100 Å before. The cobalt-molybdenum containing catalyst (MB-592), after calcination at 500 °C gives microcrystalline TiO_2 anatase (average particle diameter = 226 Å) as main crystalline phase, with, in addition, some $CoMoO_4$ and possibly minor amounts of $Co_2Mo_3O_8$, CoO and Co_3O_4. SEM shows that the crystallites are loosely packed into plate-like agglomerates which seem to break apart upon calcination. The ^{119}Sn Mössbauer spectroscopic study of used catalysts (runs # 115, 116 and 123) mixed with solid residues and high molecular weight

hydrocarbons, before and after homogeneization, showed that the relative amounts of tin(II) and tin(IV) had not changed significantly, therefore oxidation of stannous tin to stannic tin does not occur during homogeneization. A variable temperature Mössbauer study of twelve tin "titanate" catalysts was carried out in the range 15-300 K, in order to determine more accurately Sn(II) and Sn(IV) relative amounts by reducing the difference between their recoil-free fraction. It was found that all the tin(II) contained in non-calcined unused samples had oxidized to tin(IV) in the time that elapsed since the Mössbauer spectrum was taken at RT [G. Denes, "Characterization of Tin Catalysts by Mössbauer Spectroscopy, Final Report to DSS, SN # OST85-00243, 1987]. It is concluded that the surprisingly low amount of tin(II) we observed previously by RT Mössbauer spectroscopy was due to the oxidation of most of the tin(II) initially present in the catalysts to tin(IV) that had been taking place in the solid since they were prepared, therefore tin(II) must be located on the surface of the titanate particles, and as a result, it is readily available for reaction with atmospheric oxygen. We recommend that the samples be prepared in deoxygenated solutions, and stored in an oxygen free environment. Variable temperature Mössbauer spectroscopy showed the importance of lattice strength and temperature on the recoil-free fraction, and the resulting necessity to account for this in quantitative analysis by the Mössbauer technique, if large errors in relative amounts of different tin species in a mixture are to be avoided. The tin(II) chloride supported on coal was entirely oxidized to tin(IV) and was coordinated by a mixture of Cl and O ligands. Its lattice is much softer (Debye temperature ~ 300 K) and it nearly escapes detection at RT. The amount of SnS formed in the hydroprocessing reaction is mostly a function of the ease of cleavage of the Sn-ligand bonds, and since the Sn-Cl bonds are much more labile than the Sn-O bonds, tin chloride supported on coal produces much more SnS than the titanates.

RESUME

Le but du travail de recherche présenté dans ce rapport était la caractérisation de catalyseurs à l'étain ou au cobalt-molybdène, supportés sur un squelette titane-oxygène. Les catalyseurs ont été préparés par le Dr. Jacques Monnier, Laboratoires de Recherche sur l'Energie, Centre Canadien de la Technologie des Minéraux et de l'Energie, Energie, Mines et Ressources Canada, qui nous les a fournis. Une grande partie de ce travail a été consacrée à des études supplémentaires d'échantillons déja caractérisés sous un contrat précédent [G. Denes, "Characterization of Tin Catalysts by Mössbauer Spectroscopy, Final Report to DSS, SN # OST85-00243, 1987]. L'étain 119 a été utilisé comme sonde locale des sites de l'étain en spectroscopie Mössbauer, afin de déterminer le degré d'oxidation de l'étain sur ces sites, d'évaluer les proportions relatives d'étain divalent et tétravalent, d'étudier l'environnement de l'étain et d'identifier la nature des phases qui en contiennent. La diffraction de rayons X sur poudres a montré si les échantillons étaient cristallins, microcristallins ou amorphes, et quand des pics de Bragg sont observés, les phases cristallines ont été identifiées et le diamètre moyen des particules des phases microcristallines a été estimé. La texture des catalyseurs solides, ainsi que la forme et taille des particules, ont été déterminées par microscopie électronique à balayage (SEM). Nous avons observé que tous les échantillons étaient amorphes ou microcristallins avant calcination. La calcination entraîne une croissance des particules, cependant, les échantillons calcinés sont toujours microcristallins, avec un diamètre moyen des particules compris entre 100 et 350 Å après calcination, alors qu'avant il est toujours inférieur à 100 Å. Les catalyseurs au cobalt-molybdène (MB-592), après calcination à 500 °C, contiennent TiO_2 microcristallin, principalement sous la forme anatase (diamètre moyen des particules = 226 Å), avec en plus, une petite quantité d'au moins une autre

phase microcristalline dont probablement $CoMoO_4$, ainsi que, peut-être, $Co_2Mo_3O_8$, CoO et Co_3O_4. La microscopie électronique montre que les cristallites forment des agglomérats friables, dont certains ressemblent à des plaquettes, et qui semblent se désintégrer en poudre fine après calcination. L'étude par spectroscopie Mössbauer de ^{119}Sn des catalyseurs à l'étain après utilisation (tests # 115, 116 et 123), mélangés avec les résidus solides et les hydrocarbures lourds, avant et après homogénéisation, a montré que les proportions relatives d'étain divalent et tétravalent ne changent pas au cours de l'homogénéisation, par conséquent, l'oxydation de l'étain stanneux en étain stannique ne se produit pas au cours de l'homogénéisation du mélange. L'étude de douze catalyseurs à l'étain par spectroscopie Mössbauer en fonction de la température a été effectuée entre 15 et 300 K, afin de déterminer avec plus de précision les quantités relatives d'étain(II) et (IV), par réduction de la différence entre la fraction résonnante sans recul de chaque espèce aux basses températures. Nous avons constaté que tout l'étain divalent contenu précédemment dans les échantillons non utilisés et non calcinés, s'était oxidé en étain tétravalent pendant l'intervalle de temps écoulé entre les mesures effectuées à température ambiante et celles à basses températures [G. Denes, "Characterization of Tin Catalysts by Mössbauer Spectroscopy, Final Report to DSS, SN # 0ST85-00243, 1987]. Par conséquent, nous concluons que la faible (étonnamment faible) quantité d'étain divalent que nous avions observée précédemment par spectroscopie Mössbauer, était en grande partie dûe à l'oxydation de la plupart de l'étain(II) présent initialement dans les catalyseurs en étain(IV), qui se déroulait dans les catalyseurs solides depuis leur préparation. Il s'en suit que l'étain(II) est probablement localisé à la surface des particules de titanate, et est donc aisément disponible pour l'oxydation par l'oxygène atmosphérique. En conclusion, nous recommandons que les échantillons soient préparés en solutions déoxygénées et stockés à l'abri de l'air et

de l'oxygène. La spectroscopie Mössbauer en fonction de la température a montré la grande importance de la rigidité du réseau cristallin et de la température sur la valeur de la fraction résonnante sans recul, et la nécessité qui en résulte de tenir ce phénomène en compte au cours d'analyses quantitatives par la technique Mössbauer afin d'éviter de larges erreurs dans les quantités relatives de différents types d'étain dans un mélange. Le chlorure d'étain divalent supporté sur charbon était entièrement oxydé en étain tétravalent, et était coordiné par un mélange de ligandes Cl et O. Son réseau est beaucoup plus mou (température de Debye ~ 300 K) si bien que son spectre est à la limite de détectibilité à température ambiante. La quantité de SnS formée dans les tests de catalyse est principalement une fonction de la facilité de clivage des laisons étain-ligandes, et puisque les liaison Sn-Cl sont plus faciles à couper que les liaisons Sn-O, le catalyseur au chlorure d'étain supporté sur charbon produit beaucoup plus de sulfure stanneux que les catalyseurs sur titanates.

INTRODUCTION

An in-depth understanding of the mechanism of catalyzed reactions requires a complete characterization of the solid phases present in the catalysts. The identification of these phases, their physical state (degree of crystallinity, particle shape and size) and the knowledge of the nature of the active sites (substituents, oxidation state, coordination, hybridization) are of prime importance. The research described below was undertaken in order to answer some of the above questions about catalysts prepared by Dr. J. Monnier in the Energy Research Laboratories, Canada Centre for Mineral and Energy Technology (CANMET), Energy, Mines and Resources Canada (EMR).

In an effort to use the large deposits of coal and bitumen or heavy oils from Western Canada for the preparation of synthetic fuels, tin and cobalt-molybdenum catalysts supported on hydrous "titanates"* were recently prepared at CANMET for coprocessing reactions, yielding higher coal conversion and oil yield as well as improved product quality (1-4). The general synthetic procedure of the catalysts was the same as that developped at the Sandia National Laboratories of the U. S. Department of Energy (5-7), which consists in precipitating the hydrous titanate support by hydrolysis of a titanium(IV) compound, followed by deposition of the appropriate metal onto the support by ion exchange. The samples were analyzed, characterized using some techniques, and tested at CANMET Energy Research Laboratories; then, some of them, at different stage of preparation or use, were sent to us for study by X-ray powder diffraction, ^{119}Sn Mössbauer spectroscopy and/or electron microscopy. Most of the

---

*We use here the name "titanate", even though there is no structural evidence that discrete titanate ions exist in these materials. Dosch, Stephens and Stohl first called this support "hydrous titanate" (5-7) and Cotton and Wilkinson (8) also use the name "titanate" for similar materials.

tin-containing catalysts underwent a preliminary characterization in our laboratory (3, 9-11).

The samples we have characterized in our laboratory at Concordia University are listed in Table I. For easy and quick reference, each sample was assigned a code number, JM1 to JM31, as shown in Table I. The history of each sample and the relationships between some of them are given on fig. 1.

The catalysts supported on hydrous titanate were prepared in CANMET laboratories as described in (1-3), using the general method described by Dosch, Stephens and Stohl (5-7). The catalyst support was produced by reacting titanium(IV) isopropoxide with a cold solution of sodium hydroxide (15% wt) in methanol, which yields a soluble intermediate compound. Then, this liquid is treated with a mixture of 10 wt % water in acetone, which results in the precipitation of hydrous sodium "titanate", $NaTi_2O_5H$. After washing and drying the precipitate under vacuum, a white fluffy powder is obtained. Two batches of sodium hydrous titanate support (1st generation, JM13, and 2nd generation, JM14) were prepared and used to prepare the catalysts. If the solution of NaOH used is at RT, precipitation of a white gel in a mother liquor is obtained, instead of a soluble intermediate. The gel is treated as follows: (i) in one case, it is washed with methanol and filtered (solid JM29), (ii) and in another case, the gel was filtered without washing (solid JM30). Then, both solids were dried to give the final JM29 and JM30 samples. In the next step, the metal exchanged hydrous titanate (MEHT) catalysts were obtained by ion exchange of sodium with the appropriate metal in an aqueous solution of the metal ion. A solution of stannous chloride dihydrate, $SnCl_2.2H_2O$, was used for the preparation of the tin catalysts. As shown in fig.1, MB-585 (JM10) and MB-586 (JM7) are obtained by ion exchange from the 1st generation support (JM13) while MB-599 (JM9) is obtained from the

Table I: List of Samples Studied

JM1: MB-587 non-calcined catalyst obtained from the 1st generation support (JM13), after dissolution of the support, by coprecipitation with Sn.

JM2: MB-586 calcined catalyst, obtained by ion exchange (JM7) from the 1st generation support (JM13), then calcination.

JM3: MB-585 calcined catalyst, obtained by ion exchange (JM10) from the first generation support (JM13), then calcination.

JM4: Run #54, with calcined MB-586 catalyst (JM2) obtained by ion exchange (JM7) from the 1st generation support (JM13).

JM5: MB-590 (Sn/Coal): tin deposited on coal Forestburg C, from $SnCl_2.2H_2O$.

JM6: Run #55, with calcined MB-587 catalyst (JM8) obtained by coprecipitation with Sn (JM1) from the 1st generation support (JM13).

JM7: MB-586 non-calcined catalyst obtained by ion exchange from the 1st generation support (JM13).

JM8: MB-587 calcined catalyst, obtained by coprecipitation with Sn (JM1) from the 1st generation support (JM13), then calcination.

JM9: MB-599 non-calcined catalyst obtained by ion exchange from the 2nd generation support (JM14).

JM10: MB-585 non-calcined catalyst obtained by ion exchange from the 1st generation support (JM13).

JM11: Run #63, with calcined MB-599 catalyst (JM19) obtained by ion exchange (JM9) from the 2nd generation support (JM14).

JM12: Run #76, with non-calcined MB-599 catalyst (JM19) obtained by ion exchange (JM19) from the 2nd generation support (JM14).

JM13: 1st generation support.

JM14: 2nd generation support.

JM15: Calcined 2nd generation support.

JM17: Coal Forestburg C (92.2 % vitrinite).

Table 1: continued 1

JM19: Calcined MB-599 catalyst (JM9) obtained by ion exchange from the 2nd generation support (JM14).

JM20: Run # 115, catalyst MB-590 mixed with solid residues and heavy hydrocarbons, before homogeneizing.

JM21: Run # 116, catalyst MB-590 mixed with solid residues and heavy hydrocarbons, before homogeneizing.

JM22: Run # 123, catalyst MB-599 mixed with solid residues and heavy hydrocarbons, before homogeneizing.

JM23: MB-592, Co-Mo catalyst, supported on hydrous titanate, calcined at 150 °C.

JM24: MB-592, Co-Mo catalyst, supported on hydrous titanate, calcined at 350 °C.

JM25: MB-592, Co-Mo catalyst, supported on hydrous titanate, calcined at 500 °C.

JM26: Run # 115, catalyst MB-590 mixed with solid residues and heavy hydrocarbons, after homogeneizing.

JM27: Run # 116, catalyst MB-590 mixed with solid residues and heavy hydrocarbons, after homogeneizing.

JM28: Run # 123, catalyst MB-599 mixed with solid residues and heavy hydrocarbons, after homogeneizing.

JM29: In the preparation of hydrous titanate support: Precipitate obtained when Ti(IV) isopropoxide is added to a solution of wt 15% NaOH in methanol at RT, then washed with methanol and filtered.

JM30: Same precipitate as for JM29, except it is filtered immediately after precipitation (no washing).

JM31: Run # 52 (THF insoluble) with catalyst MB-590.

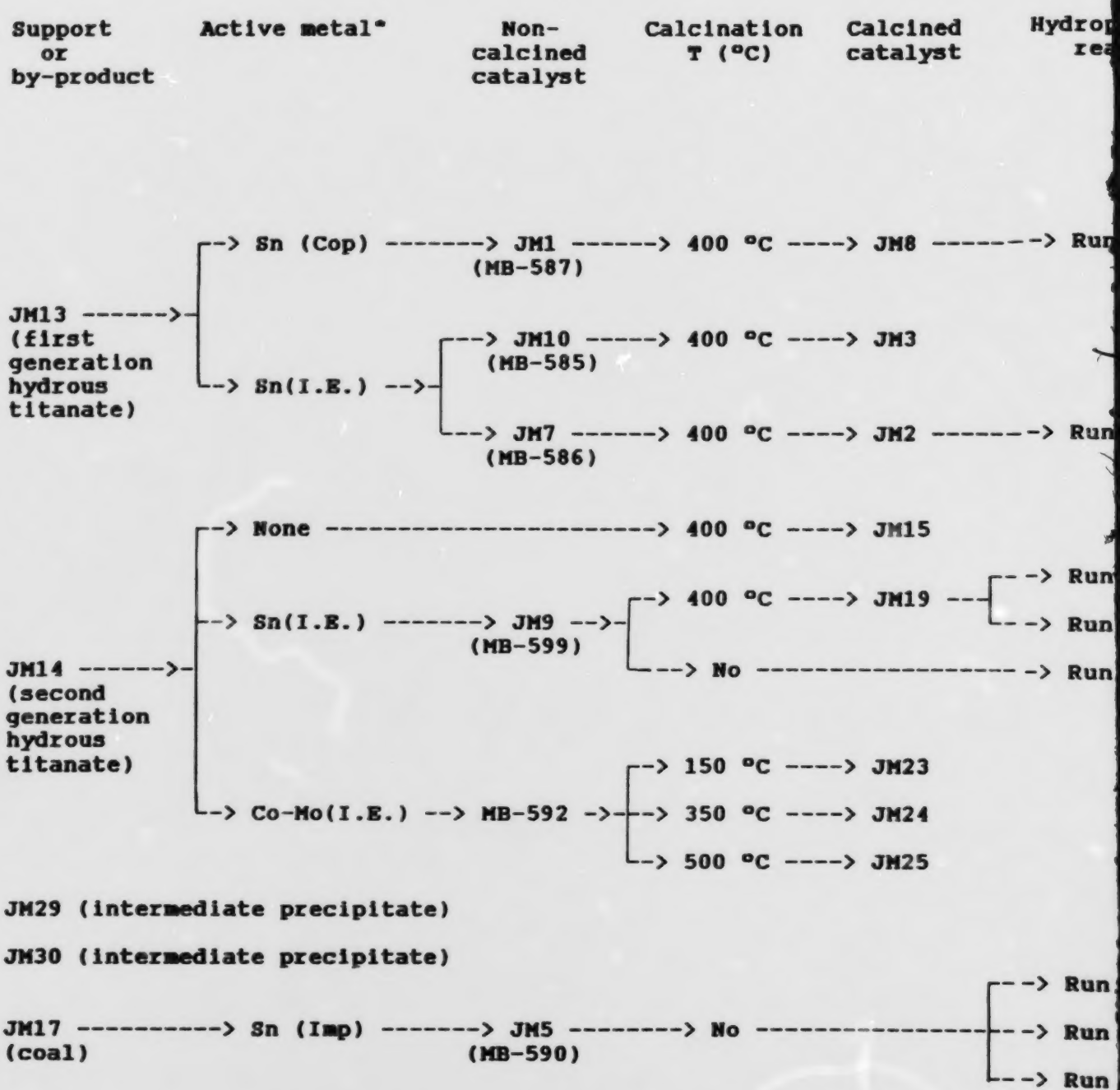

*Cop= coprecipitation, I.E.= ionic exchange, Imp= impregnation.

Figure 1: Diagram of samples history.

T.23440-6-9097

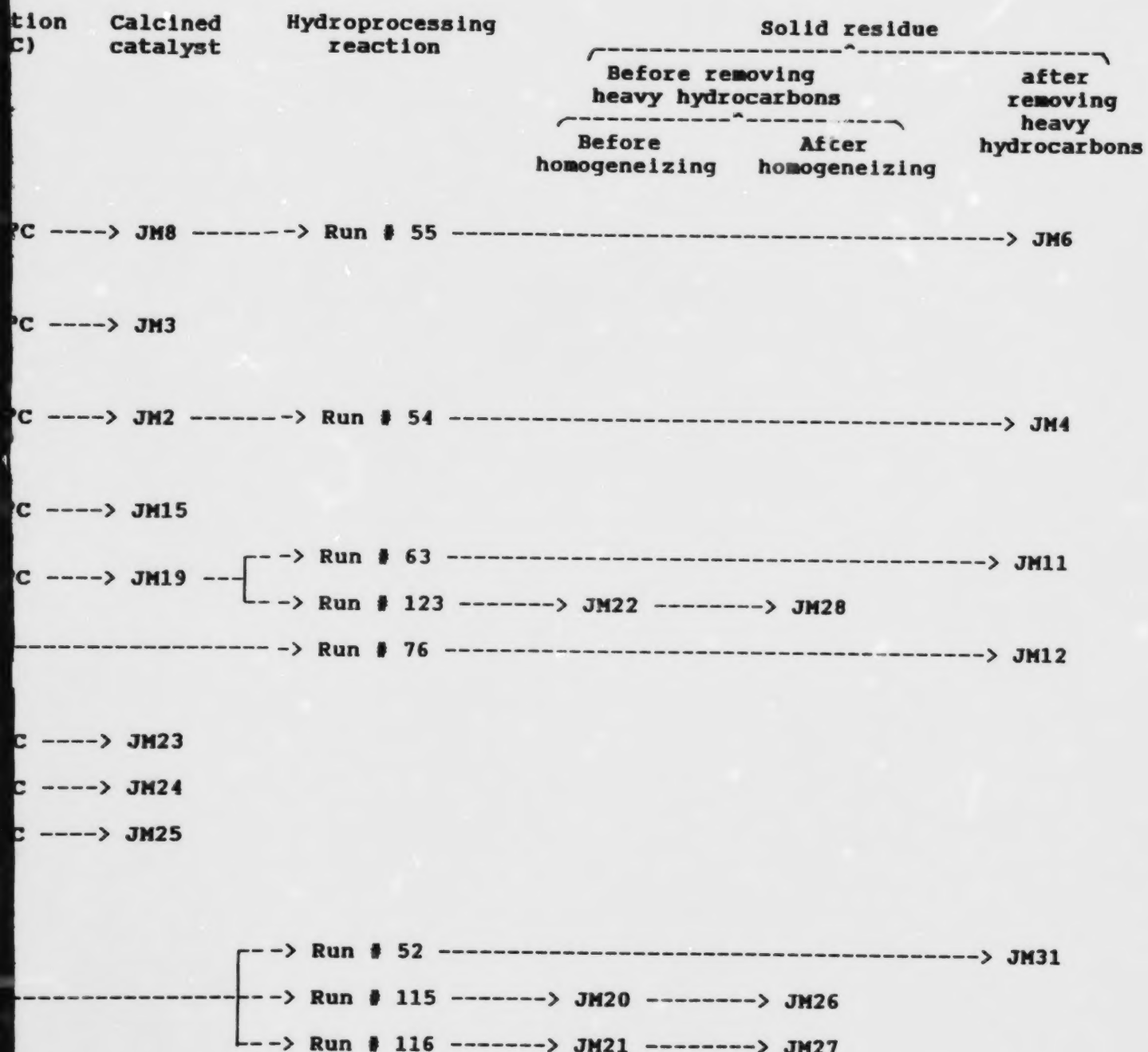
tion
C)
Calcined catalyst
Hydroprocessing reaction
Solid residue
Before removing heavy hydrocarbons
after removing heavy hydrocarbons
Before homogeneizing
Afcer homogeneizing
C ----> JM8 ------> Run # 55 ----------> JM6
C ----> JM3
C ----> JM2 ------> Run # 54 ----------> JM4
C ----> JM15
C ----> JM19 ---> Run # 63 ----------> JM11
---> Run # 123 -------> JM22 --------> JM28
----------> Run # 76 ----------> JM12
C ----> JM23
C ----> JM24
C ----> JM25
---> Run # 52 ----------> JM31
----------> Run # 115 -------> JM20 --------> JM26
---> Run # 116 -------> JM21 --------> JM27

regnation.

s history.

2nd generation support (JM14), using the same technique. In one case, the 1st generation support dissolved in the tin dichloride solution. Raising the pH by addition of ammonium hydroxide resulted in precipitation of a yellow solid (JM1) which strongly smelled ammonia even after washing and drying. As the titanium and tin solid species were simultaneously obtained on addition of ammonia, the solid obtained (JM1) was called "coprecipitated catalyst".

The last step of the preparation consisted in calcining the samples. Calcination of the tin catalysts was carried out in air at 400 °C for two hours. This gave the samples JM8, JM3, JM2 and JM19, which where obtained upon calcination of JM1, JM10, JM7 and JM9, respectively. JM15 is the 2nd generation support (JM14), not metal exchanged, heated in the same conditions. The batch of Co-Mo catalyst (MB-592) was split into four parts, which were calcined in air at 150 °C (JM23), 350 °C (JM24), 400 °C (not sent to me) and 500 °C (JM25), respectively (4).

The sample JM5 (Sn/coal) was prepared by impregnation of Forestburg subbituminous C coal (92.2 % vitrinite, 64.04 wt % carbon and 20.41 wt % oxygen, "dry basis") in an aqueous solution of stannous chloride dihydrate, $SnCl_2.2H_2O$. After filtering and washing, the sample was dried at RT under vacuum.

The catalytic hydroprocessing tests and their results have already been described (1-4). A mixture of catalyst, subbituminous coal and heavy oil was heated at 410 °C for 225 min in an autoclave at 3.4 MPa pressure, under continous hydrogen flow of 275 mL/min. A cold trap removed all the distillates from the outlet gases during the reaction. After reaction, all the liquids were drained, and the remaining solid (residue + catalyst) was washed with pentane, toluene and THF (tetrahydrofuran) to remove the oil, asphaltenes and

preasphaltenes. The THF insoluble solid consists mainly of the catalysts residue, the coke formed, as evidenced by petrographic analysis (1) and eventually, some unreacted coal. I was provided with five THF insoluble residues: JM6 (run #55 with calcined MB-587), JM4 (run #54 with calcined MB-586), JM11 (run #63 with calcined MB-599), JM12 (run #76 with non-calcined MB-599) and JM31 (run # 52 with MB-590). I was also provided with three residues (runs # 115, 116 and 123) not separated from the heavy hydrocarbons, for Mössbauer spectroscopic tests at RT before homogeneizing (JM20, JM21 and JM22, respectively) and after homogeneizing (JM26, JM27 and JM28, respectively). Homogeneization was carried out by gentle heating in order to decrease the viscosity of the heavy hydrocarbons.

Altogether, I received from CANMET twenty eight samples:
(i) two gels obtained in the preparation of the support (JM29 and JM30),
(ii) two titanate supports (JM13 and JM14),
(iii) one calcined support (JM15),
(iv) four non-calcined catalysts (JM1, JM7, JM9 and JM10),
(v) seven calcined catalysts (JM2, JM3, JM8, JM19, JM23, JM24 and JM25),
(vi) three residues mixed with heavy hydrocarbons before homogeneizing (JM20, JM21 and JM22), which were returned after homogeneizing (JM26, JM27 and JM28),
(vii) five THF insoluble residues (JM4, JM6, JM11, JM12 and JM31), and
(viii) one tin catalyst supported on coal (JM5).
Details about each sample can be found in Table I and in fig. 1.

In order to do a meaningful interpretation of my measurements, it was necessary to know the chemical composition of the samples. Furthermore, for the Mössbauer spectroscopic measurements, it is useful to know in advance the tin content in

the sample as the amount of sample used for the measurement depends on the amount of tin it contains. Indeed, an insufficient amount results in a very weak (and therefore inaccurate) spectrum or no spectrum at all. On the other hand, if the amount of sample is too large, line broadening (thus poor resolution) is observed, and in severe cases, the gamma count rate is too low, because of excessive non-resonant absorption, and results in a very weak spectrum. Table II gives relevant analytical results for several of the samples. When no results are given, they were not available to me. Two analytical techniques, viz. Inductive Coupled Argon Plasma Spectrometry (ICAPS) and Neutron Activation (NA) were used for bulk analysis. The MB-592 catalyst (JM23, JM24 and JM25) was also analyzed for the surface composition, using X-ray Photoelectron Spectroscopy (XPS). Table II gives the results for Ti, Sn, Na, Co and Mo. Sodium was the only significant contaminant in the tin containing catalyst. No analytical data for sodium were available for the bulk analysis of the Co-Mo catalysts, however, no sodium was detected at the surface. A low sodium level indicates that the ion exchange was complete, while for high contamination, possible formation of sodium titanates or sodium stannates has to be considered. The results in Table II are given in weight % metal oxide (TiO_2, SnO_2 or Na_2O) for the ICAPS results and weight % metal (Ti, Sn, Co, Mo or Na) for NA and XPS results. While the Ti and Sn results are similar for both techniques, as shown by similar Ti/Sn ratios, the sodium content is much higher for neutron activation than for ICAPS. This leads to Na/Sn and Na/Ti ratios which are about one order of magnitude higher for the neutron activation results. According to ICAPS analyses, the highest Na/Sn ratio is found for JM19 (Na/Sn=0.14). On the other hand, NA results indicate Na/Sn ratios are close to 0.5 for JM2 and JM3, over 1 for JM19 and equal 5 for JM8. If these high ratios are to be believed, formation of large amounts of sodium stannates is possible. On the other hand, if sodium titanates were formed, it would be only in small amounts as the

Table II: Some Analytical Results for the Samples Investigated

(1) Cat.	(2) O or M	(3) S or B	(4) Anal. Tech.	(5) TiO_2 or Ti	(6) MO_n or M	(7) MoO_3 or Mo	(8) Na_2O or Na	(9) Ti/M or C/Sn	(10) Ti/Mo	(11) Na/M	(12) Na/Ti	(13) Co/Mo
JM1	O	B	ICAPS	80.65	10.21	-	-	14.57	-	-	-	-
JM2	M	B	NA	43.2	12.7	-	1.08	8.18	-	0.45	0.06	-
JM2	O	B	ICAPS	76.92	16.05	-	0.35	8.82	-	0.03	0.003	-
JM3	M	B	NA	48.2	9.00	-	1.14	12.63	-	0.63	0.05	-
JM3	O	B	ICAPS	80.12	12.91	-	0.38	11.22	-	0.03	0.003	-
JM4	O	B	ICAPS	-	1.97	-	-	-	-	-	-	-
JM5	M	B	-	-	-	-	-	-	-	-	-	-
JM6	O	B	ICAPS	-	0.8	-	-	-	-	-	-	-
JM7	O	B	ICAPS	75.11	14.40	-	-	9.5	-	-	-	-
JM8	M	B	NA	42.4	3.48	-	3.52	29.67	-	5.00	0.11	-
JM8	O	B	ICAPS	89.82	6.35	-	0.53	28.50	-	0.10	0.004	-
JM9	-	-	-	-	-	-	-	-	-	-	-	-
JM10	-	-	-	-	-	-	-	-	-	-	-	-
JM11	O	B	ICAPS	-	3.32	-	-	-	-	-	-	-
JM12	O	B	ICAPS	-	2.45	-	-	-	-	-	-	-
JM13	-	-	-	-	-	-	-	-	-	-	-	-
JM14	-	-	-	-	-	-	-	-	-	-	-	-
JM15	-	-	-	-	-	-	-	-	-	-	-	-
JM19	M	B	NA	36.5	16.8	-	3.86	5.43	-	1.22	0.22	-
JM19	O	B	ICAPS	58.32	33.16	-	3.59	3.36	-	0.14	0.04	-

Table II: Continued

(1) Cat.	(2) O or M	(3) S or B	(4) Anal. Tech.	(5) TiO_2 or Ti	(6) MO_n or M	(7) MoO_3 or Mo	(8) Na_2O or Na	(9) Ti/M	(10) Ti/Mo	(11) Na/M	(12) Na/Ti	(13) Co/Mo
JM20	-	-	-	-	-	-	-	-	-	-	-	-
JM21	-	-	-	-	-	-	-	-	-	-	-	-
JM22	-	-	-	-	-	-	-	-	-	-	-	-
JM23	M	S	XPS	39.2	7.6	9.0	0	6.33	8.71	0	0	1.37
JM24	M	S	XPS	38.7	7.8	11.3	0	6.11	6.90	0	0	0.89
JM25	M	S	XPS	36.7	10.5	12.6	0	4.33	5.89	0	0	1.36
JM25??	M	B	????	40.5	5.0	10.1	-	10.09	7.93	0	0	0.79
JM26	-	-	-	-	-	-	-	-	-	-	-	-
JM27	-	-	-	-	-	-	-	-	-	-	-	-
JM28	-	-	-	-	-	-	-	-	-	-	-	-
JM29	-	-	-	-	-	-	-	-	-	-	-	-
JM30	-	-	-	-	-	-	-	-	-	-	-	-
JM31	-	-	-	-	-	-	-	-	-	-	-	-

Codes for the column of the tables:

(1) Cat.= catalyst number.

(2) O or M: O= oxide, M= metal; neutron activation (NA) results are given in metal weight (%) whereas the ICAPS results are given in metal oxide weight %, and the XPS results in atomic %.

(3) S or B: S= surface analysis, B= bulk analysis.

(4) Anal. Tech.= analytical technique: NA= neutron activation, ICAPS= Inductive coupled argon plasma spectroscopy, XPS= X-ray photoelectron spectroscopy.

(6) MO_n= SnO_2 (or CoO for JM23, JM24 and JM 25).

(6) and (9) M= Sn (or Co for JM23, JM24 and JM25).

highest Na/Ti neutron activation result is Na/Ti=0.22 for JM19, while the ICAPS values are negligible. As a consequence of the analytical results available to me, I concluded that sodium may be present in sufficient quantity to form large amounts of sodium stannates and small amounts of sodium titanates. X-ray diffraction and Mössbauer data were checked for the formation of such species. For MB-592, surface and bulk analyses are in fairly good agreement, however, the Ti level seems higher in the bulk, which indicate that Co and Mo are deposited on the surface of the Ti-O framework. The absence of sodium at the surface indicates that the ionic exchange was complete. The Co/Mo ratio close to one indicates that stoichiometric compounds such as $CoMoO_4$ could be formed, and this was checked by X-ray diffraction.

Table III identifies the techniques used in this project for the study of the twenty seven samples. All tin-containing catalysts were studied by Mössbauer spectroscopy at RT. In addition, twelve tin containing samples were also studied by Mössbauer spectroscopy versus temperature (12-300 K); that is more than the seven to ten samples required by the terms of the contract. The four remaining tin catalysts (JM19, JM26, JM27 and JM28) will also been studied as a function of temperature. These could not be done before the deadline for writing this report because of the long time required for data accumulation (almost one month per sample for 13 temperatures, plus at least 3 days for changing the sample. In addition, measurements were delayed by a total of one year, by three major breakdowns, one requiring the instrument being sent back to the factory in the U.S.A. X-ray powder diffraction was performed on all samples, with the exception of the residues mixed with heavy hydrocarbons (JM20, JM21, JM22, JM26, JM27 and JM28). Scanning electron microscopy was used for the supports and all non-used catalysts (non-calcined and calcined). No electron micrographs were taken for residues after the tests because it would be hard to see the used

Table III: Techniques Used to Study the Samples

0= not used
1= used in the first part of this study (9)
2= used in this work
3= being done although not required by the contract
RT= room (ambient) temperature
LT= low temperature

Samples	^{119m}Sn Mössbauer Spectroscopy		X-ray Powder Diffraction	Scanning Electron Microscopy
	RT	LT		
JM1	1	2	1	1
JM2	1	2	1	1
JM3	1	2	1	1
JM4	1	2	1	0
JM5	2	2	1	0
JM6	1	2	1	0
JM7	1	2	1	1
JM8	1	2	1	1
JM9	1	2	1	1
JM10	1	2	1	1
JM11	1	2	1	0
JM12	1	2	1	0
JM13	0	0	1	1
JM14	0	0	1	1
JM15	0	0	1	1
JM19	1	3	1	0
JM20	2	0	0	0
JM21	2	0	0	0
JM22	2	0	0	0
JM23	0	0	2	2
JM24	0	0	2	2
JM25	0	0	2	2
JM26	2	3	0	0
JM27	2	3	0	0
JM28	2	3	0	0
JM29	0	0	2	0
JM30	0	0	2	0
JM31	2	0	0	0

catalysts which were intimately mixed with a large amount of coke or unreacted coal or heavy hydrocarbons.

In the following sections, I give:
(i) the basic theory of the Mössbauer effect and recoil-free fraction, and the dependence of the recoil-free fraction on temperature and the nature of the solid,
(ii) the experimental techniques (equipment, experimental procedures);
(iii) the results of the analyses performed and a dicussion of the results;
(iv) the general conclusions, and
(v) the recommendations based on my observations.

THEORY OF THE MÖSSBAUER EFFECT AND THE RECOIL-FREE FRACTION

This section describes briefly the theory of the Mössbauer effect and the influence of temperature and lattice strength on the recoil-free fraction. This is necessary for understanding the reason for the low temperature study of the catalysts. The reader can find more details on the theory of the Mössbauer effect and Mössbauer spectroscopy in ref. 12 & 13.

1. RECOIL ENERGY AND THERMAL BROADENING.

Let us consider an isolated atom in the gas phase, in a nuclear excited state. E_g is the nuclear energy in the ground state, E_e in the excited state, and E_t, the transition energy, is the difference:

$$E_t = E_e - E_g \qquad (I)$$

The atom in the nuclear excited state is moving at a velocity V. When the nucleus decays to the ground state, it emits a γ-photon of energy E_γ. At the same time, its velocity changes by a value of v, the "recoil velocity" (like a gun when it is fired). Let us examine the energetics of the system before and after γ-emission (Table IV).

Table IV: Energetics of γ-ray Emission and Absorption

	Before emission	After emission
Nuclear level	Excited	Ground
Nuclear energy	E_e	E_g
Nuclear velocity	V	V+v
Total energy (nucleus + γ-photon)	$E_e + MV^2/2$	$E_\gamma + E_g + M(V+v)^2/2$
Total momentum (nucleus + γ-photon)	MV	$M(V+v) + E_\gamma/c$

Note: c= velocity of light.

Energy and momentum are conserved in the γ-emission process. By conservation of energy:

$$E_e + MV^2/2 = E_\gamma + E_g + [M(V+v)^2]/2 \quad \text{(II)}$$

Recalling that $E_t = E_e - E_g$, the difference (δE) between the energy of the nuclear transition (E_t) and the energy of the emitted γ-photon (E_γ) is:

$$\delta E = E_t - E_\gamma = Mv^2/2 + MvV \quad \text{(III)}$$

or $$\delta E = E_R + E_D \quad \text{(IV)}$$

with $E_R = Mv^2/2$ is the "recoil kinetic energy" (V)

and $E_D = MvV$ is the "Doppler effect energy". (VI)

The statistical energy distribution of the emitted γ-ray by a gas is shown on fig. 2a (fig. 2 is taken from ref. 13, p. 6). There is a broad Gaussian distribution of γ-ray energy. The linewidth is $2\overline{E}_D$ and the maximum of the peak is shifted by E_R from E_t, towards lower energies. Similarly, the energy distribution for absorption of a γ-photon is a broad Gaussian (linewidth= $2\overline{E}_D$) shifted from E_t by E_R towards higher energies (fig. 2b).

2. THE MÖSSBAUER EFFECT.

Because of the shift of the emission and absorption of γ-ray energies in opposite directions, no successive resonant emission and reabsorption of a γ-photon is theoretically possible. However, because of large thermal broadening, there is the possibility of a weak zone of overlap between the two distributions, where successive emission and reabsorption can be possible (fig. 2c). However, the zone of overlap disappears at low temperature because of line narrowing (less thermal broadening), and it becomes lost in the background at higher temperatures because of its weakness and broad distribution.

The uniqueness of the Mössbauer effect is that it provides a mean of eliminating the destructive effects of both the recoil and thermal broadening. In a solid, the atoms, and therefore the nuclei, are no longer isolated and animated of a brownian motion.

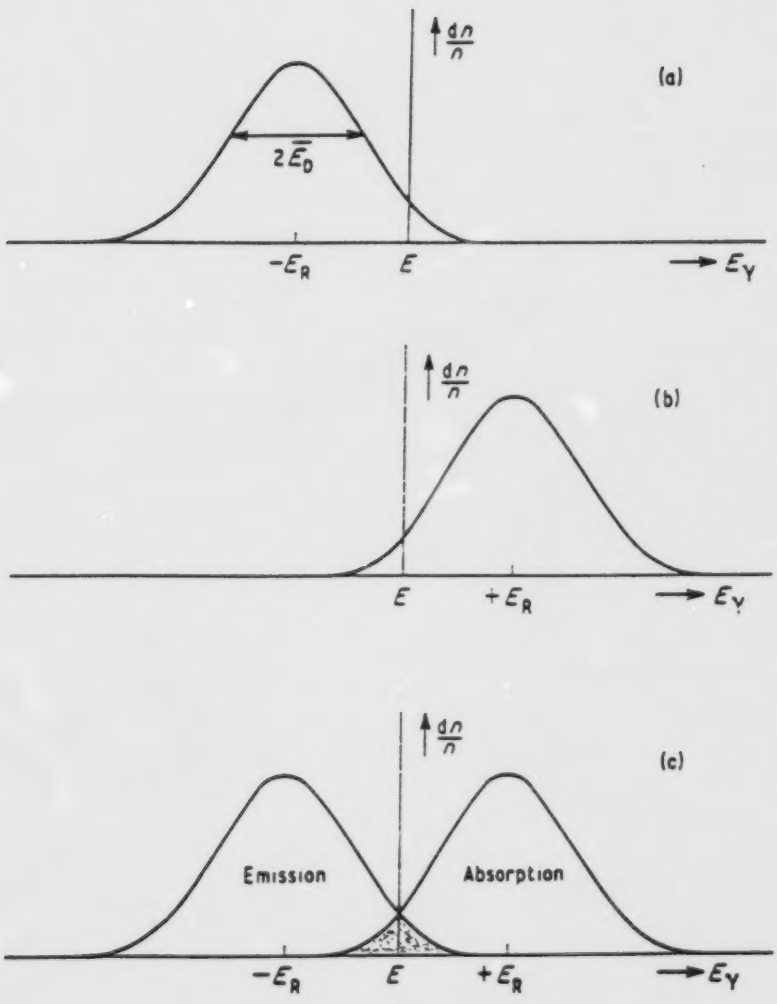

Figure 2: Statistical distribution in the γ-ray energy for (a) emission, (b) absorption, and (c) resonant overlap for successive emission and absorption.

Instead, they are imbedded in fixed positions of a solid bonding network and cannot move independently of the whole solid.

Table V: Typical Energies for Nuclear and Chemical Interactions
(from ref. 13, p. 4)

Mössbauer γ-ray (E_γ)	$10^6 - 10^7$	kJ mol^{-1}
Chemical bonds and lattice energies	$10^2 - 10^3$	kJ mol^{-1}
Lattice vibrations	$0.5 - 5$	kJ mol^{-1}
Nuclear recoil and Doppler broadening (E_R, E_D)	$10^{-2} - 1$	kJ mol^{-1}
Heisenberg linewidths (Γ_n)	$10^{-7} - 10^{-4}$	kJ mol^{-1}

As can be seen from Table V, the recoil energy is much less than the chemical bond and lattice energies, and therefore recoil cannot break bonds or displace atoms from their lattice site. On the other hand, recoil energies are similar in magnitude with lattice vibration energies. If the recoil energy is transferred directly to the lattice vibrational energy, then the γ-ray energy is still degraded. However, the lattice vibrational energy is quantized, and each quantum is called a "phonon". Therefore, the recoil energy can only be transferred to the lattice if it corresponds closely to an allowed quantum jump. These are integral multiples of $\hbar w$, i.e. $0, \pm\hbar w, \pm 2\hbar w, \ldots$, where $\hbar = h/2\pi$ (h= Planck's constant) and w= lattice vibrational frequency.

For emission of γ-rays by a solid, only the fraction f_m of emission events result in no transfer of energy to the lattice, i.e. "zero-phonon transition", and the fraction $(1 - f_m)$ transfers one phonon of energy hw to the lattice. Then

$$E_R = (1 - f_m)\hbar w \quad \text{or} \quad f_m = 1 - E_R/\hbar w \qquad \text{(VII)}$$

f_m is called the "recoil-free fraction" or "recoiless fraction" of the γ-ray source. Similarly, for γ-ray absorption, the fraction f_m, called recoil-free fraction or recoiless fraction of the absorber, results in a zero-phonon process.

$$E_R = (1 - f_m)\hbar w \quad \text{or} \quad f_m = 1 - E_R/\hbar w \qquad \text{(VIII)}$$

Since in Mössbauer spectroscopy, only zero-phonon emission and

absorption of γ-rays are useful, only the fraction ($f_a \times f_a$) of the nuclear events gives rise to a Mössbauer spectrum. The zero-phonon process does not suffer from thermal broadening (since there is no recoil, the recoil velocity v is zero, therefore the recoil energy E_D defined in equation VI is also zero), and the resonant emission and absorption of γ-rays follows a Lorentzian distribution, of which width is limited only by Heisenberg's natural linewidth (Table V) and the source and absorber homogeneity.

3. EFFECT OF TEMPERATURE AND LATTICE STRENGTH ON THE RECOIL-FREE FRACTION.

During the course of the study reported here, the same γ-ray source was used, therefore, f_a was a constant. On the other hand, f_a changes with the nature of the tin containing phase and the temperature of the samples when the Mössbauer spectra were recorded.

3.1. Effect of lattice strength.

A strong lattice (high melting covalent or ionic compounds) have a high lattice vibrational frequency, and therefore, equation VIII leads to a large value of the recoil-free fraction. On the other hand, a low melting solid, with weak bonds, has a lower vibrational frequency, and as a consequence, a lower recoil-free fraction. For example, let us compare the case of divalent tin and tetravalent tin (fig. 3). In tetravalent tin oxides, such as SnO_2 and the similar pseudo-octahedral stannic tin oxide found in the catalysts (3 & 9-11), tin(IV) is rigidly held in a strong three-dimensional network of tin-oxygen bonds, therefore, this type of tin compound has a high recoil-free fraction. In contrast, divalent tin possesses a non-bonding lone pair of electrons which is located on a non-bonding orbital in the tin valence shell. This results in a lower coordination number, most of the time three (14, 15), sometimes four (16-19),

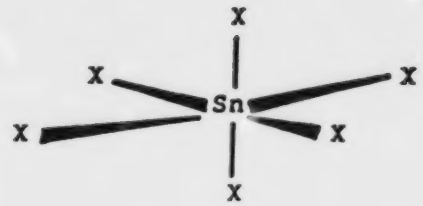

Sn(IV): SnX_6 Octahedron
(Example: SnO_2)

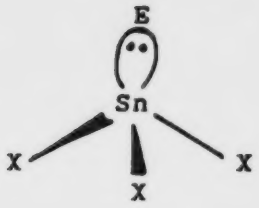

Sn(II): SnX_3E pseudotetrahedron
(Example: Sn(1) in α-SnF_2)

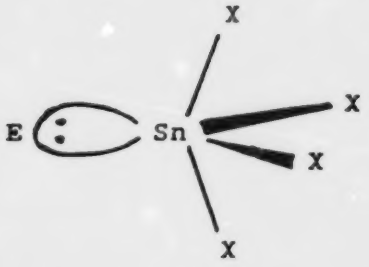

Sn(II): SnX_4E pseudotrigonal bipyramid (Example: γ-SnF_2)

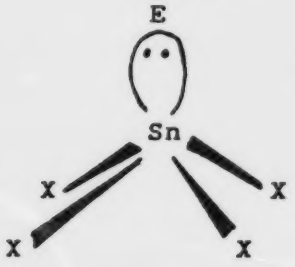

Sn(II): SnX_4 square prism
(Example: SnO, $PbSn_4F_{10}$)

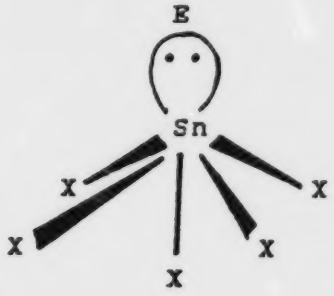

Sn(II): SnX_5E pseudooctahedron
(Example: α-$PbSnF_4$ type, Sn(2) in α-SnF_2)

Figure 3: Coordination of tin(IV) and tin(II) in inorganic ionic and iono-covalent solids (X= anion, E= lone pair).

and very rarely five (19-21). The lower coordination and lone pair repulsions with other anions result in departure from three-dimensionality. Indeed, real two-dimensional structures can be found, like in black SnO (16) and in the α-$PbSnF_4$ type (21). However, even when the overall structure is three-dimensional, there is a local interruption in bonding in the direction of the tin(II)-lone pairs axis. This results in a weaker bonding, and as a result, the recoil-free fraction is lower. The effect of non-equal recoil-free fractions for the components of a mixture is <u>not</u> minor and can result in a totally erroneous estimation of their relative abundance in the mixture. For example, at RT, the recoil-free fraction of SnO_2 [$f_a(SnO_2)$= 0.44] (22), and α-SnF_2 [$f_a(\alpha\text{-}SnF_2)$= 0.034] (23) differ by more than one order of magnitude. It results that the Mössbauer signal of SnO_2 in a mixture of SnO_2 and α-SnF_2 is about 13 times as strong as if their recoil-free fraction were the same, and in ignoring this effect, its abundance in the mixture would be grossly overestimated (24). Further, liquids and gases have a lattice strength of zero (since the atoms or molecules are not held together in a solid lattice), and therefore a recoil-free fraction of zero, which results in no Mössbauer effect.

3.2. <u>Effect of temperature: recoil-free fraction and Debye-Waller factor</u>.

Above, we used the concept of "<u>Einstein solid</u>", with a single lattice vibration frequency w (often called w_m= <u>Einstein frequency</u>). Einstein solid is a useful concept for explaining the quantization of phonons, however, it is an oversimplification of real solids (25). The "<u>Debye solid</u>" is more realistic, since it includes frequencies ranging from zero to a maximum value, w_D, the "<u>Debye frequency</u>". Fortunately, the very low frequencies are difficult to excite, otherwise, the Mössbauer effect would not exist.

In the Debye model, the recoil-free fraction of an absorber is $f_a = 1 - E_R/\hbar w_D$ (IX)
A characteristic temperature, called θ_D= Debye temperature, is defined as follows: $\hbar w_D = k_B \theta_D$ (X)
with k_B= Boltzmann constant.
The Debye temperature θ_D for metals varies from 80 K for lead (soft lattice) to 1,000 K for beryllium (hard lattice), but it is very difficult to estimate it for heteroatomic compounds. Therefore, it is almost impossible to compute recoil-free fractions from thermodynamic data.

Integration over w= 0 to w_D in the Debye model leads to the following equation, which gives the recoil-free fraction f versus temperature T:

$$f = \exp\left[\frac{-6E_R}{k_B\theta_D}\left\{\frac{1}{4} + \left(\frac{T}{\theta_D}\right)^2 \int_0^{\theta_D/T} \frac{x\,dx}{e^x-1}\right\}\right] \qquad (XI)$$

This is also often written as $f = e^{-2W}$ (XII)
where W is often loosely called "Debye-Waller factor", or more adequately "Lamb-Mössbauer factor". The Debye-Waller factor is obtained from X-ray or neutron diffraction experiments. However, again, accurate determination of Debye-Waller factors is difficult. It must be done from single crystal diffraction data, and requires extensive corrections using parameters difficult to obtain and the theory of the corrections is not completely understood. Furthermore, the Debye-Waller factor is anisotropic, i.e. it is a symmetric tensor of rank 2 (maximum of 6 numbers), instead of a scalar number. Moreover, diffraction techniques and Mössbauer spectroscopy do not probe the lattice thermal vibrations the same way, especially averaging over time and over lattice sites are not done the same way, and as a result, they usually lead to different values. The problem is so difficult that only few successful approaches have been published

(26-28).

Equation XI cannot be used as such, however it can be simplified, depending on the relative values of θ_D and T:

- at absolute zero (0 K): $$f = \exp\left[\frac{-3E_m}{2k_m\theta_D}\right] \qquad \text{(XIII)}$$

- at low temperatures ($T<<\theta_D$):

$$f = \exp\left[\frac{-E_m}{k_m\theta_D}\left\{\frac{3}{2} + \frac{\pi^2T^2}{\theta_D^2}\right\}\right] = \exp[K_1T^2] \qquad \text{(XIV)}$$

- in the high temperature limit ($T>\theta_D/2$):

$$f = \exp\left[\frac{-6E_mT}{k_m\theta_D^2}\right] = \exp[K_2T] \qquad \text{(XV)}$$

with K_1 and K_2 being constants.

The variation of the recoil-free fraction with temperature is shown on fig. 4. The following is observed:
(i) Even at absolute zero (zero point motion), the recoil-free fraction is larger for strong lattices than for weak lattices, however, it is always lower than unity;
(ii) ln f versus T is a parabola at low temperatures (zone A on fig. 4);
(iii) ln f versus T is a linear function at higher temperatures (zone B on fig. 4);
(iv) ln f versus T is a parabola as T ---> θ_D, because of the more pronounced anharmonicity of the thermal vibrations at high temperatures (29) (zone C on fig. 4). The recoil-free fraction falls abruptly to zero, i.e. the Mössbauer spectrum disappears, as T ---> θ_D.

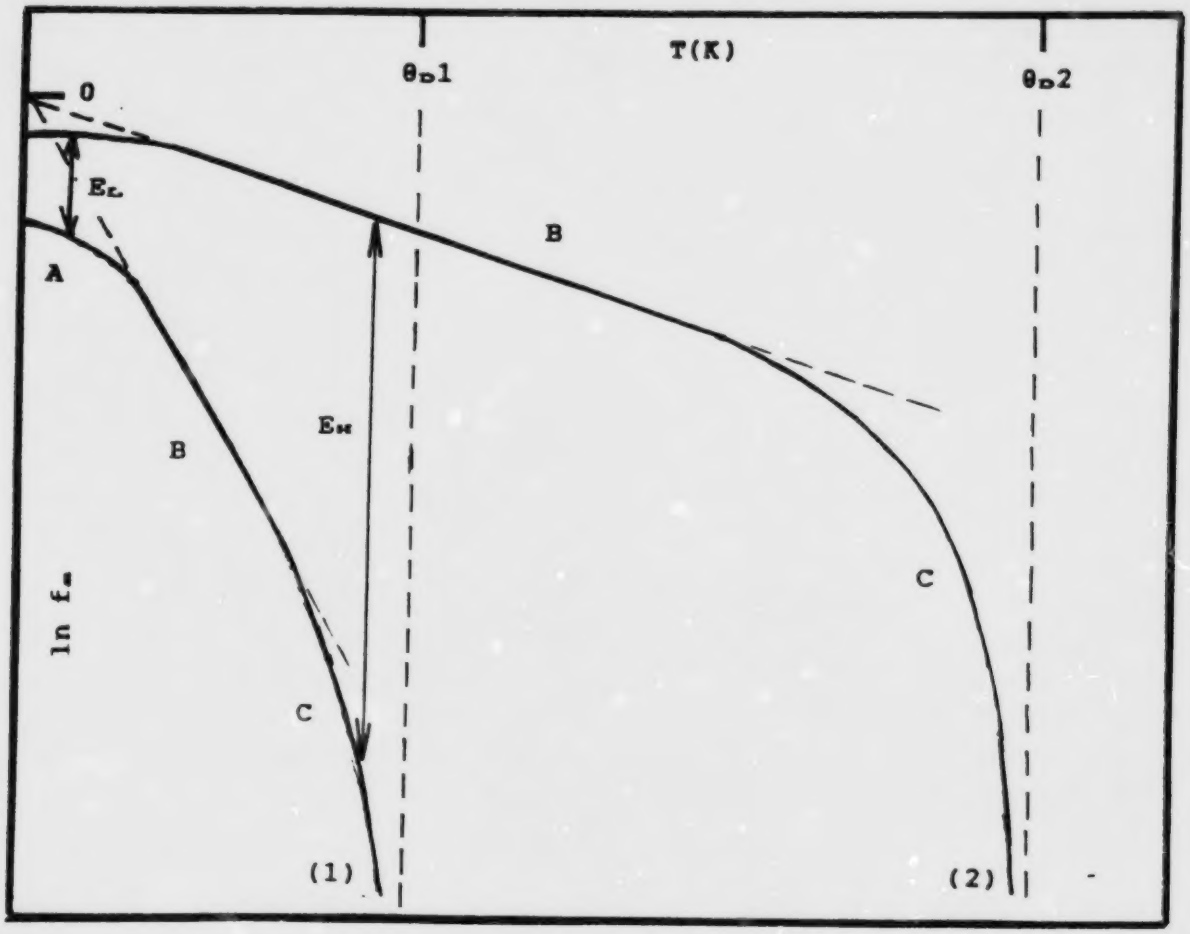

Figure 4: Evolution of the recoil-free fraction with temperature as a function of lattice strength.

A= Zero point motion
B= Harmonic thermal vibrations
C= Anharmonic thermal vibrations
E_L= Difference between the recoil-free fractions of a soft lattice and a hard lattice at low temperature
E_H= Difference between the recoil-free fractions of a soft lattice and a hard lattice at high temperature
f_a= Absorber recoil-free fraction
θ_D1, θ_D2= Debye temperature of compound (1) and (2), respectively.
(1) Soft lattice compound
(2) Hard lattice compound.

3.3. Use of variable temperature Mössbauer spectroscopy for quantitative analysis of mixtures.

When a solid contains a mixture of phases, its Mössbauer spectrum is the sum of the spectrum of each component which contain the Mössbauer nuclide being probed. For example, let us consider a catalyst that contains N_D atoms of divalent tin and N_T atoms of tetravalent tin. Its Mössbauer spectrum gives a subspectrum for divalent tin of intensity I_D, and a subspectrum for tetravalent tin of intensity I_T. One could expect the intensity of each of their subspectra in the total spectrum of the mixture to be proportional to their relative abundance, i.e.

$$I_D \propto N_D \quad \text{and} \quad I_T \propto N_T \qquad \text{(XVI)}$$

However, this does not hold because their "sensitivity", i.e. their recoil-free fraction, are not the same. We have shown in section 3.1. (page 29) above that ignoring the difference in recoil-free fraction can result in values of relative abundance that are totally erroneous. If we call $(f_a)_D$ and $(f_a)_T$ the recoil-free fraction of divalent and tetravalent tin, respectively, one finds that

$$I_D \propto (f_a)_D * N_D \quad \text{and} \quad I_T \propto (f_a)_T * N_T \qquad \text{(XVII)}$$

In order to calculate N_D and N_T from measured values of I_D and I_T, one must know first $(f_a)_D$ and $(f_a)_T$. As explained above, recoil-free fractions (or Debye-Waller factors) cannot be calculated from measurements done using other techniques. In addition, they are also difficult to calculate accurately from Mössbauer spectroscopic data, and it requires measurements done on pure phases, for each phase in turn (12). Furthermore, values obtained for crystalline phases would not be useable for microcrystalline phases, which are known to have a lower recoil-free fraction if the crystallites are sufficiently small (30); this is particularly important for the present catalysts, which have been shown to be microcrystalline, especially before calcination, when tin(II) is present, the crystallites are often so small as to escape detection by X-ray diffraction (3, 9-11).

The best way to carry out a quantitative analysis is to make a calibration curve, using physical mixtures of the concerned phases in variable proportions. Care has to be taken to use standards with controlled particle size. This method cannot be applied in the case of the catalysts under study for the following reasons:

- the samples are microcrystalline, with variable particle sizes;
- no pure sample of each tin containing phase is available, and even their nature is unclear, especially for the non-calcined samples, which would be the samples that would benefit most from this analysis, since they are the only samples to contain tin(II) oxide mixed with tin(IV) oxide.

An alternative technique is to record the Mössbauer spectrum versus temperature, starting at very low temperatures. Fig. 4 shows that the recoil-free fraction for a soft lattice decreases much more rapidly than that of a hard lattice when temperature increases. The following is observed as temperature is decreased:

(i) At very high temperature ($T>\theta_D2$), no Mössbauer spectrum is observed and one can mistakenly think that the sample contains no Mössbauer nuclide;

(ii) For $\theta_D1<T<\theta_D2$, only the spectrum of compound (2) is observed, and one gets the false impression that there is no compound (1) in the mixture;

(iii) For $0\ K<<T<\theta_D1$, one sees a mixture of (1) and (2), however, the abundance of (1) is grossly underestimated: E_H is the error in the relative amounts of (1) and (2) at high temperature (i.e. far above 0 K);

(iv) At very low temperatures (at the zero point motion), the recoil-free fractions for soft and hard lattices are much closer to each other and the error (E_L) on their relative abundance is

much smaller. The two following points must be noted:

- even at 0 K, the recoil-free fraction is higher for the hard lattice (due to equation XIII), therefore the problem is not totally eliminated, however it is very strongly reduced;
- it is not necessary to cool to 0 K, since the recoil-free fractions do not change much with temperature at very low temperatures.

Variable temperature Mössbauer spectroscopy is the method that we have used in an attempt to estimate the relative amounts of tin(II) and tin(IV) in the catalysts.

EXPERIMENTAL

1. SAMPLE MANIPULATION

All samples were fine powders. The color of the catalysts was yellow, light yellow or white while the THF insoluble residues were black, as listed in Table VI. All samples seemed unreactive to air at room temperature and therefore were handled in air with no special precaution.

2. SCANNING ELECTRON MICROSCOPY

The samples for electron microscopy were ground and dried in air at ca. 120°C overnight to remove adsorbed water. Then they were stored in a dessicator. A small amount of each sample was sprinkled on a 0.5 inch diameter aluminum stub for electron microscopy, to which a sticky tab had previously been applied. The excess powder was removed by shaking and blowing a gentle breeze of nitrogen on the stub. Gold coating was applied in a vacuum deposition system to avoid electric charge build-up during electron irradiation, which would cause focusing problems. The micrographs were taken using a polaroid camera on a Hitachi S-520 scanning electron microscope operating with the filament energized at 15kV.

3. X-RAY POWDER DIFFRACTION

All X-ray diffraction patterns were run on finely ground powders which were packed in a plexiglass holder, using a glass microscope slide, then mounted at the center of the goniometer of a Philips PW1050-25 X-ray powder diffractometer. The K-alpha radiation of Cu (1.54178 Å) was used, the K-beta line being filtred by a Ni foil filter. The scans were run at a speed of 0.5° (θ) .min^{-1} in the range 3-40° (θ). Tests at lower speeds did not provide higher accuracy because of large linewidth and strong peak overlapping. The powder patterns were recorded on chart paper as the intensity of diffracted X-ray beam versus the

Table VI: Experimental Parameters for Mössbauer Runs

Sample	Color	Holder	sample mass(mg)	mass Sn/cm²(mg)
JM1	yellow	teflon	643	17.2
JM2	pale yellow	Al	237	10.0
JM3	yellow	Al	295	10.0
JM5	black	Al	1,937	-
JM4	black	Al	1,935	10.0
JM6	black	Al	3,132	6.6
JM7	creme	teflon	300	11.4
JM8	light yellow	Al	600	10.0
JM9	light yellow	teflon	300	-
JM10	light creme	teflon	600	-
JM11	black	Al	1,147	10.0
JM12	black	Al	1,955	10.0
JM13	white	-	-	-
JM14	white	-	-	-
JM15	white	-	-	-
JM19	white	teflon	302	26.3
JM20	dark brown	Al	6,107	-
JM21	dark brown	teflon	7,800	-
JM22	dark brown	teflon	7,716	-
JM23	greenish grey	-	-	-
JM24	greyish green	-	-	-
JM25	greenish brown	-	-	-
JM26	dark brown	teflon	6,107	-
JM27	dark brown	teflon	7,800	-
JM28	dark brown	teflon	7,783	-
JM29	white	-	-	-
JM30	white	-	-	-
JM31	black	Al	3,050	-

angle (θ) between the surface of the sample and the incident X-ray beam. An alpha-SnF_2 standard sample was run before and after each pattern for checking the line positions. This was also used as standard for linewidth, for correcting the observed line broadening from the instrumental broadening in the determination of average particle size.

4. MÖSSBAUER SPECTROSCOPY

Mössbauer spectra were recorded on a Mössbauer spectrometer that I purchased and set up at Concordia University. The 23.875 KeV Mössbauer gamma-ray line was obtained using a 15 mCi $Ca^{119m}SnO_3$ source purchased from Amersham. The Doppler velocity was provided by an Elscint driving system including a MVT-4 velocity transducer, a MFG-N-5 function generator and a MDF-N-5 driver generator, powered from a EG&G ORTEC NIM-BIN, and operating in the triangle mode. The 25.04 and 25.27 KeV X-ray lines were removed using a 0.1 mm thick palladium foil filter. The gamma-rays were recorded using a Harshaw power supply and Na(Tl)I scintillation counter operating at 900 V. The samples were finely ground powders, generally in the amount necessary to give 10mg $Sn.cm^{-2}$, based on the analytical data of Table II. This amount is sufficient to give a strong resonant gamma-ray absorption, yet well below saturation level. In some cases (JM1,JM7 and JM19), this amount was found to be insufficient and it was increased. In the case of JM6, as there was not a sufficient amount of the sample to have 10 mg $Sn.cm^{-2}$, the whole sample was used, corresponding to 6.6 mg $Sn.cm^{-2}$, which was enough to give a good Mössbauer spectrum. When no analytical data was available (JM5, JM9, JM10, JM20, JM21, JM22, JM26, JM27, JM28 and JM31), the amount to be used was estimated by comparison with similar samples, which gave good results.

Neat samples were loaded into polytetrafluoroethylene (teflon) or aluminum holders with a tightly fitting screw cap .

Both sample holder and cap have a thin window of 3 cm^2 area. The sample holders are fitted inside a 1 cm thick wall brass cylinder which is fitted at the top a 2 cm thick wall lead cylinder for shielding purposes. The source was vibrated inside the lead cylinder, along the cylinder axis. The lead cylinder, with the brass holder containing the teflon sample holder mounted on its top, was mounted on the top of the velocity transducer, and the whole thing was resting on the vibration-free table, in the vertical position. The source and absorber must be protected against all sources of external vibrations such as pumps, fans from electrical appliances, etc..., so common in research laboratories. Indeed, gamma-ray modulation is done by Doppler effect, i.e. by moving the source relative to the absorber. The Doppler modulation, in the case of ^{119}Sn Mössbauer spectroscopy, is in the range -8 to +8 $mm.s^{-1}$ source velocity, which corresponds to common frequencies of vibrations of pumps and fans. External sources of vibration would therefore distort the gamma-ray modulation, resulting in significant line broadening and thus serious loss of resolution. Protection against external vibrations is provided by having the transducer, thus the source, and the absorber on the vibration-free table. The table is a large aluminum plate (310x105x2cm^3) sustained by six legs attached to ciment blocks which are immersed in three sand boxes which are protected from the floor by a thick rubber sheet which provides a damping of the vibrations. The vibrations not stopped by the rubber are absorbed by the sand. All electrical parts of the spectrometer that have a fan for cooling and therefore are sources of vibrations, i.e. the multichannel analyzer, the NIM-BIN and the high voltage power supply, are mounted on a four-wheeled rack resting on the floor, with no physical connections to the vibration-free parts, except flexible electrical cables. This arrangement works well as no significant instrumental line broadening was detected. The source to detector distance was maintained at 16 cm . This, combined with the small amplitude

of vibration of the source provided by a transducer frequency of 22 Hz, gives spectra free of cosine broadening.

The source was maintained at room temperature for all measurements. This provides strong spectra as the recoil-free fraction of tin oxides is high for both the divalent and tetravalent oxidation states (31).

For variable temperature studies, the samples were loaded into the same teflon or aluminum holders, which were fitted very tightly into a copper clamp. The copper clamp was tightly screwed on the tip of the cryogenic unit. This ensures a good thermal contact and thermal stability and minimizes the thermal gradient within the samples. The refrigeration system was a two-stage Displex DMX-20 closed cycle helium refrigerator purchased from Air Products (APD Cryogenics Inc). It comprises the following items (fig. 5-7):

(i) A compressor: module model 1R04WSL. It is charged with 250 psi (1,724 kPa) He when the power is off. When the power is turned on, the helium pressure rises to 325 psi (2,441 kPa). The helium purity is 99.999 % or better. The compressor is located on the floor, however a spring system and rubber sheet reduces the vibrations transmitted to the floor (fig. 7).

(ii) An expander module: model CS-202 (fig. 6). It receives the high pressure helium from the compressor and drives it to the two- stage expander where the sudden expansion of the helium absorbs heat and thereby lowers the temperature (fig. 5). The low pressure helium is returned to the compressor. The expander module is rigidly attached to the wall of the building and has no rigid connection to the Mössbauer interface or to the vibration-free table (fig. 6&7). This prevents the undesired vibrations and knocking produced by the expander module from reaching the sample.

(iii) A Mössbauer interface: module model DMX-20(fig. 6).

This is a cold finger system, which is connected to the expander module by a flexible rubber bellow. The heat transfer to the expander module occurs through helium gas at slightly above atmospheric pressure. The minimum temperature at the sample area is 12 K. The temperature can be raised to any value in the range 12 - 300 K, using the 30 W heater (100C bakeable thermofoil heater) located on the cold finger, just above the sample. The temperature is measured with a chromel/gold 0.07 at. % Fe thermocouple, of which tip is indium soldered in the copper block of the cold finger, just near the sample. The Mössbauer interface is rigidly attached to the vibration-free table and has no rigid connection to the expander module or to the pumping system (fig. 7). Therefore, it is free of parasitic vibrations.

(iv) Two hoses: two hoses, made of convoluted metal tubing for flexibility, and covered with braided metal sheath, connect the compressor module to the expander (Fig. 5&7). One carries the high pressure helium to the expander, and the other returns the low pressure helium to the compressor. To prevent leaks and contamination of the high purity helium and to maintain a charged state, both ends of each hose and the compressor are equipped with self-sealing couplings.

(v) A digital temperature controller: model 3700-APE, made by Scientific Instruments Inc. It allows the control of the sample temperature in the range 12 to 300 K, with a resolution of 0.1 K and an accuracy of + or - 0.5 K.

(vi) Vacuum system: It includes the following:

- a Welch Duo-seal roughing pump, model No. 1400;
- a Bendix diffusion pump, model VHP-20-24, containing 100cm³ of silicon oil;
- an Ultek Corp. stainless steel vacuum line;
- Edwards PV 10K and PV 25K pipeline valves, clamps, rings and coseals;
- a flexible vacuum metal bellow, model FH-100-12-NWCF, purchased from Alcatel;

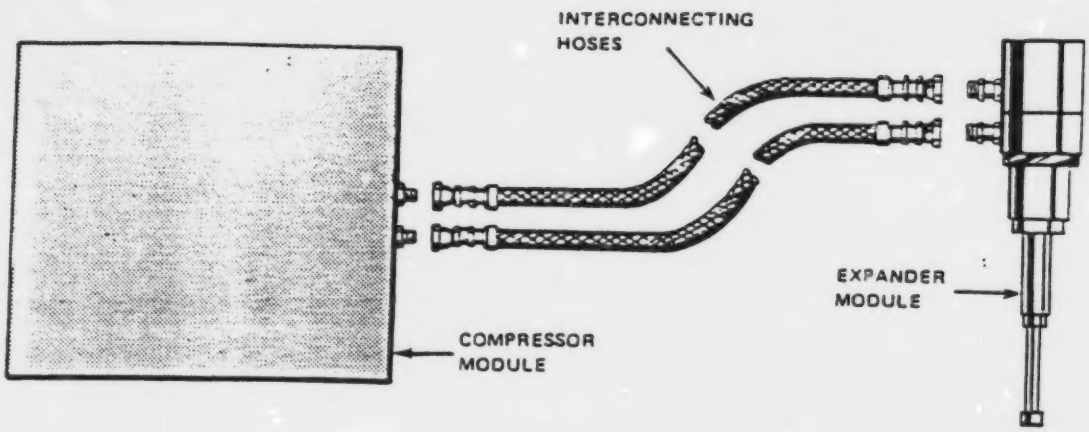

Figure 5: Air Products basic cryogenic system

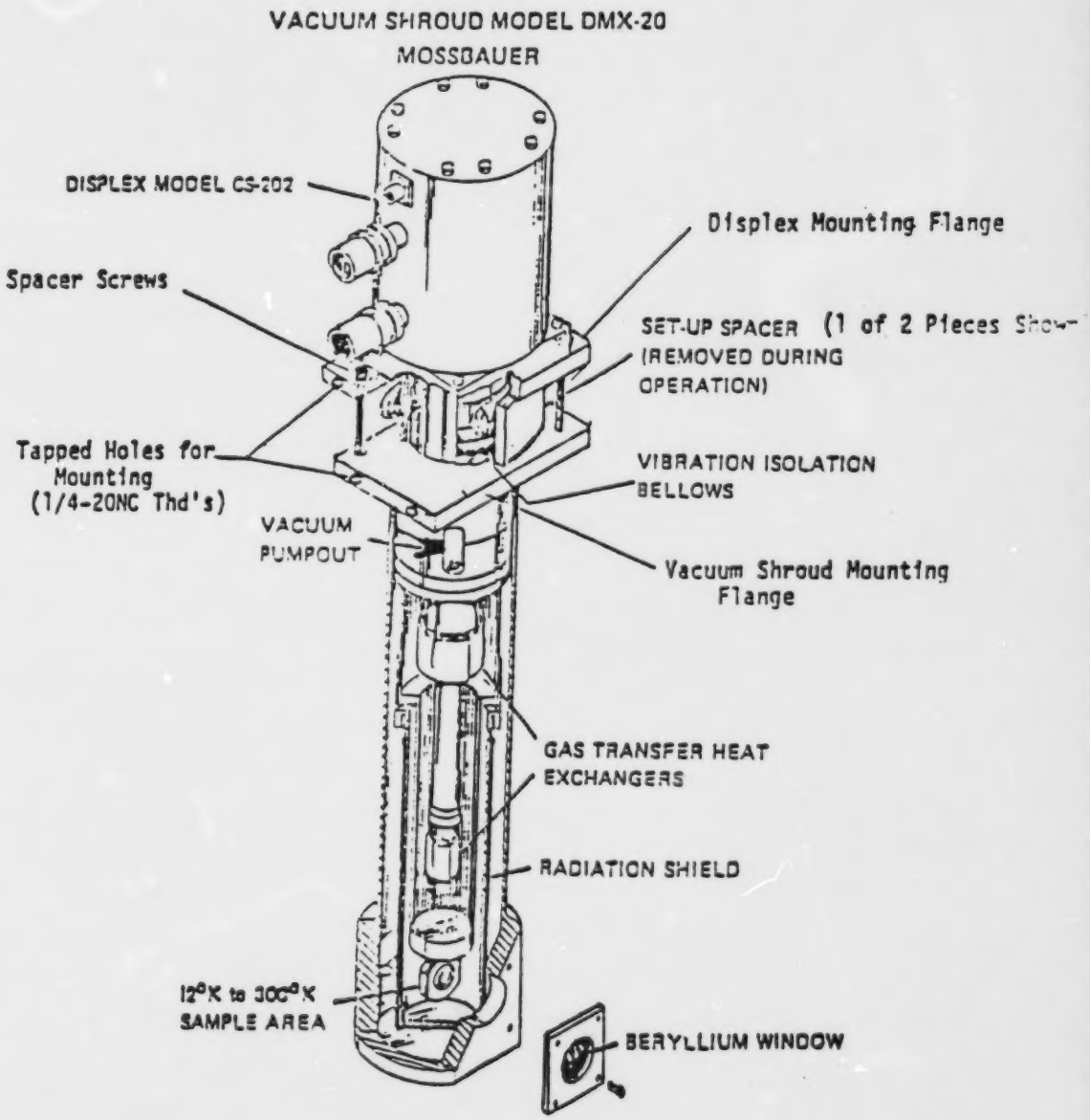

Figure 6: Air Products vacuum shroud model DMX-20 for low temperature Mössbauer spectroscopy

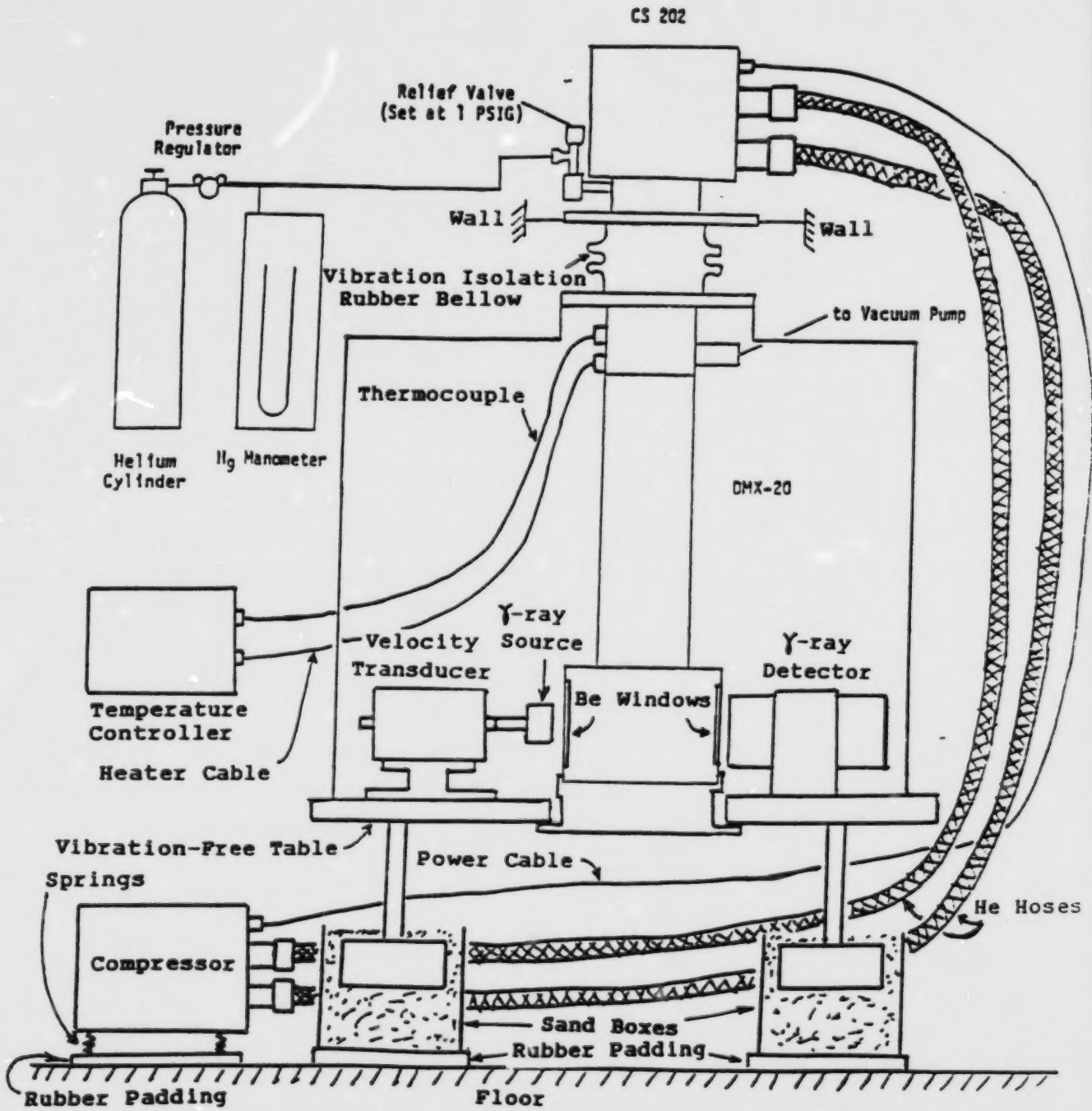

Figure 7: Set up of the Air Products Displex closed cycle helium refrigerator for low temperature Mössbauer spectroscopy

- an Alcatel P13 Pirani vacuum gauge;
- an Alcatel CF2P Penning high vacuum gauge;
- a CIT-Alcatel gauge controller, model CFA 212

The sample area is evacuated for 24 hours prior to starting the refrigeration system. The pumping system is kept running all the time, until refrigeration is stopped at the end of the experiment, and the system has warmed up to RT. The vacuum achieved is 10^{-2} to 10^{-3} mbar above liquid nitrogen temperature and 10^{-4} to 10^{-5} mbar below, as the cooling system cryopumps. The vacuum bellow cuts the vibrations from the roughing pump and the rubber bellow located between the expander module and the Mössbauer shrouds cuts the vibrations and knocking generated by the expander. Both systems are very efficient to prevent vibrations from reaching the sample area, since no noticeable linebroadening is observed. The temperature of the system is very stable (fluctuations of + or - 0.1 K). For the low temperature measurements, the velocity transducer and the gamma-ray detector are aligned horizontally with the beryllium windows of the vacuum shield of the Mössbauer shrouds, and therefore, with the sample. Perfect alignment is realized by using a Mössbauer bench, built in-house, and attached to the vibration-free-table (fig. 7). The temperatures investigated for each sample are the following (in K): 15, 35, 50, 75, 100, 125, 150, 175, 200, 225, 250, 275 and RT.

The Doppler velocity modulation was maintained in the range of -8 to +8 $mm.s^{-1}$ for studying both di- and tetravalent tin. In addition, the RT spectra were also recorded in the velocity range of -2.5 to +2.5 $mm.s^{-1}$ for a detailed study of the tin(IV) signal at room temperature, in the first part of this investigation (9).

The signal from the scintillation counter is fed into a Tracor Northern 7200 multichannel analyzer were it is amplified

by a built-in linear amplifier. Then the Mössbauer gamma-ray line is isolated in the built-in single channel analyzer. Finally, the signal is stored in a quarter (512 channels) of the 2K memory multichannel analyzer. The multichannel analyzer is operated in the multiscaling mode with the dwell time being controlled by the Elscint driving system in order to have synchronization of the source motion with the multichannel analyzer channel scanning. The spectrum is accumulated (source moving towards absorber) in the first 256 channels of the selected quarter of the memory and its mirror image (source moving away from absorber) in the next 256 channels. When the counting statistics is estimated to be sufficiently good, data acquisition is stopped and the data are transferred to an IBM compatible personal computer and stored on a diskette. Relevant experimental parameters for the Mossbauer runs are given in Table VI.

The data were calibrated using a $CaSnO_3$ and an alpha-SnF_2 standard absorbers as described in (9). The line position for $CaSnO_3$ at room temperature was taken as reference of isomer shift.

RESULTS AND DISCUSSION

1. CATALYST SUPPORTS.

1.1. Hydrous titanate support and by-products .

We showed in earlier studies (3 and 9-11), using electron microscopy and X-ray diffraction, that both JM13 and JM14 hydrous titanate supports are amorphous phases and are made of very small loosely bound particles.

The intermediate precipitate obtained in the preparation of hydrous titanate, obtained when Ti(IV) isopropoxide is added to a solution of NaOH (wt 15%) in methanol at RT, was examined by X-ray powder diffraction after filtration (JM29) and after washing with methanol then filtration (JM30). Their X-ray powder pattern, given on fig. 8, shows that the two solids are completely amorphous and show no sign of crystallinity. Therefore, one can conclude they are made of very small particles, in the lower nanometer range, i.e. their diameter is not larger than ca. 30 Å.

1.2. Coal support.

The coal Forestburg C used for the preparation of the Sn/coal catalyst was also investigated by X-ray diffraction. The lack of Bragg peaks in its powder pattern (fig. 9a) shows that it is amorphous. Only a very weak peak is observed at 3.39 Å, which can be identified as the (002) peak of hexagonal graphite, reported at 3.36 Å in the JCPDS file No. 23-64 (32). Since this is the main peak of graphite, and since it is very strongly enhanced by the high texture of graphite (preferred orientation of the layered crystallites perpendicularly to the $\vec{c}$ axis), the intensity of the (002) peak observed in coal is many orders of magnitude smaller than that of pure crystalline graphite recorded in the same conditions, therefore, the amount of crystalline graphite in the coal is very small (probably in the ppm range or lower).

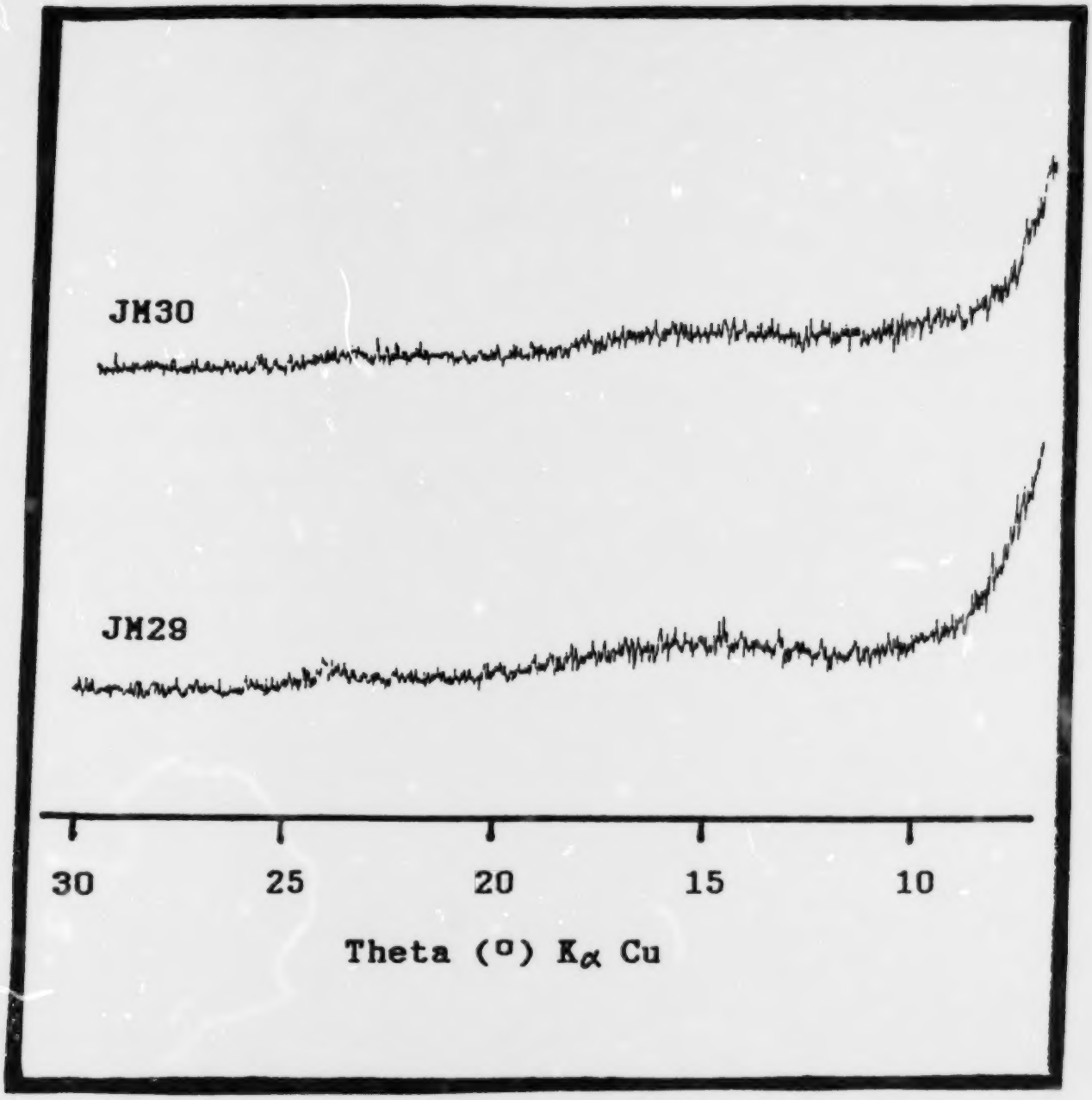

Figure 8: X-ray powder pattern of the precipitate obtained when Ti(IV) isopropoxide is added to a solution of NaOH (wt 15%) in methanol at RT, after filtration only (JM29) and after washing with methanol then filtration.

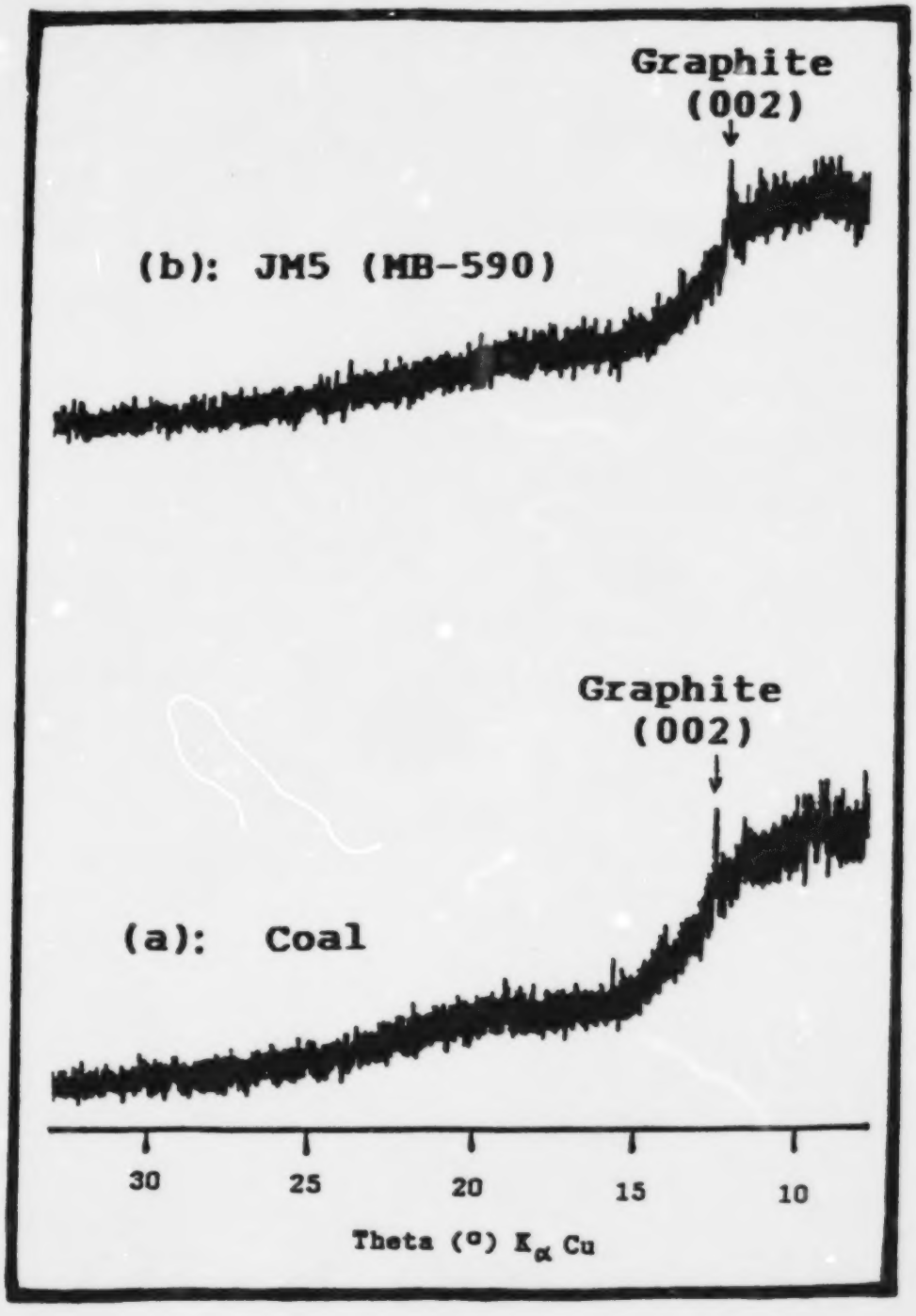

Figure 9: X-ray powder pattern of (a) Coal Forestburg C and (b) the Sn/coal catalyst (JM5).

2. NON-CALCINED CATALYSTS

2.1. Introduction.

Of the five non-calcined catalysts available to us, four of them (JM1, JM7, JM9 and JM10) are tin catalysts deposited on a hydrous titanate support by coprecipitation or ionic exchange. These were studied previously by X-ray diffraction, electron microscopy and ^{119}Sn Mössbauer spectroscopy at RT (3 and 9-11). The samples obtained by ionic exchange were shown to contain microcrystalline stannic oxide SnO_2, whereas the coprecipitated sample gave a X-ray powder pattern exhibiting minor broadening (just slightly microcrystalline) which could not be identified. Scanning electron microscopy showed that all the non-calcined catalysts are made of very small particles, loosely packed to form shapeless agglomerates with no internal structure.

2.2. Tin-impregnated coal (JM5, MB-590).

2.2.1. X-ray powder diffraction.

The X-ray powder pattern of the coal catalyst impregnated with a solution of $SnCl_2.2H_2O$ is shown on fig. 9b. The X-ray diffraction pattern is identical to that of the coal Forestburg not impregnated, i.e. only the very weak (002) peak of graphite is observed. Tin chloride loading did not result in the formation of crystalline material. Therefore, one can conclude that tin dichloride form amorphous or microcrystalline materials when deposited on coal, perhaps in the form of a thin layer located on the surface of carbon particles.

2.2.2. Ambient temperature ^{119}Sn Mössbauer spectroscopy.

The Mössbauer spectrum of coal impregnated with $SnCl_2.2H_2O$, recorded at room temperature shows surprising features:
(i) The signal is extremely weak, and is detected only after a long time of data accumulation. The maximum γ-ray absorption is only 1.1% of the background. This indicates that the tin content is very low or its recoil-free fraction at RT is very small.

(ii) The spectrum is made of a single broad peak located at +0.36 mm/s relative to $CaSnO_3$. Table VII compares the Mössbauer parameters of the catalyst with tin chlorides. The low isomer

Table VII: Ambient temperature tin-119 Mössbauer isomer shift (relative to $CaSnO_3$) and quadrupole splitting of MB-590 (JM5) coal impregnated with $SnCl_2.2H_2O$, and related compounds.

Compound	δ(mm/s)	Δ(mm/s)	Reference
MB-590 (JM5)	0.36	0	This work
$SnCl_2$	4.07	0	(12)
$SnCl_2.2H_2O$	3.55	?	(12)
$SnCl_4$	0.85	0	(12)
$SnCl_4.5H_2O$	0.25	0	(12)
SnO_2	0.00	0	(12)

shift shows that tin is tetravalent. The isomer shift is close to the value reported for tin tetrachloride pentahydrate, $SnCl_4.5H_2O$. One can suppose that tin(II) was oxidized, to some extent, by oxygen dissolved in the aqueous solution as well as oxygen that may be present on the surface on the coal particles. However, tetravalent tin may be only a minor contaminant, and one can postulate that, since recoil-free fractions for divalent tin compounds are usually much lower than those of tetravalent tin compounds with the same ligands and similar bonding, maybe most of the tin is still in the divalent state but cannot be detected because of its low recoil-free fraction at room temperature. The two problems raised above can be easily solved by low temperature Mössbauer spectroscopy.

2.2.3. Variable temperature ^{119}Sn Mössbauer spectroscopy.

Tin-119 Mössbauer spectra were recorded versus temperature in the range 15-300 K. Let us try and solve the problems raised by the ambient temperature Mössbauer spectrum:

(i) At 19.1 K, the lowest temperature achieved with this sample, the maximum γ-ray absorption is 26.5% of the background. This is a very strong signal and shows that the tin content of the sample is high enough. Therefore, the very weak spectrum, barely detectable, observed at RT was due to the low recoil-free fraction of tin, and not to an insufficient amount of tin.
(ii) The strong tin signal observed at low temperatures has the same isomer shift as that of the weak peak obtained at RT. Therefore, it is due to the same type of tin, namely tetravalent tin. No other tin signal appears at low temperature, therefore, all tin in the sample is in the tetravalent state and absence of a tin(II) signal is not due to a lower recoil-free fraction. Examination of Table IV shows that the isomer shift for JM5 falls between the values reported in the literature for SnO_2 and $SnCl_4$, therefore, it is most likely that a mixture of chlorine and oxygen ligands coordinate tin. This conclusion is reinforced by the proximity of the isomer shifts for JM5 and tin tetrachloride pentahydrate, $SnCl_4.5H_2O$. Oxidation of $SnCl_2.2H_2O$ upon impregnation on coal was complete since no divalent tin is detected, even at the lowest temperature.

The variation of the relative tin-119 Mössbauer signal with temperature is given on fig. 10. Equation XVII shows that the intensity I of the Mössbauer signal for a given site is proportional to its recoil-free fraction fa, its abundance N, and some number of physical and instrumental parameters that we group under the name K:

$$I = f_a * N * K \qquad \text{(XVIII)}$$

and $$\ln(I) = \ln(f_a) + \ln(N) + \ln(K) \qquad \text{(XIX)}$$

Since N and K are independent of temperature, ln(I) and ln(f_a) will show a similar trend in the way they vary with temperature. Figure 10 shows that the variation of the log of the relative intensity (ln I_a) for the signal of JM5 is very similar to the theoretical trend derived from the Debye model (fig. 4). The

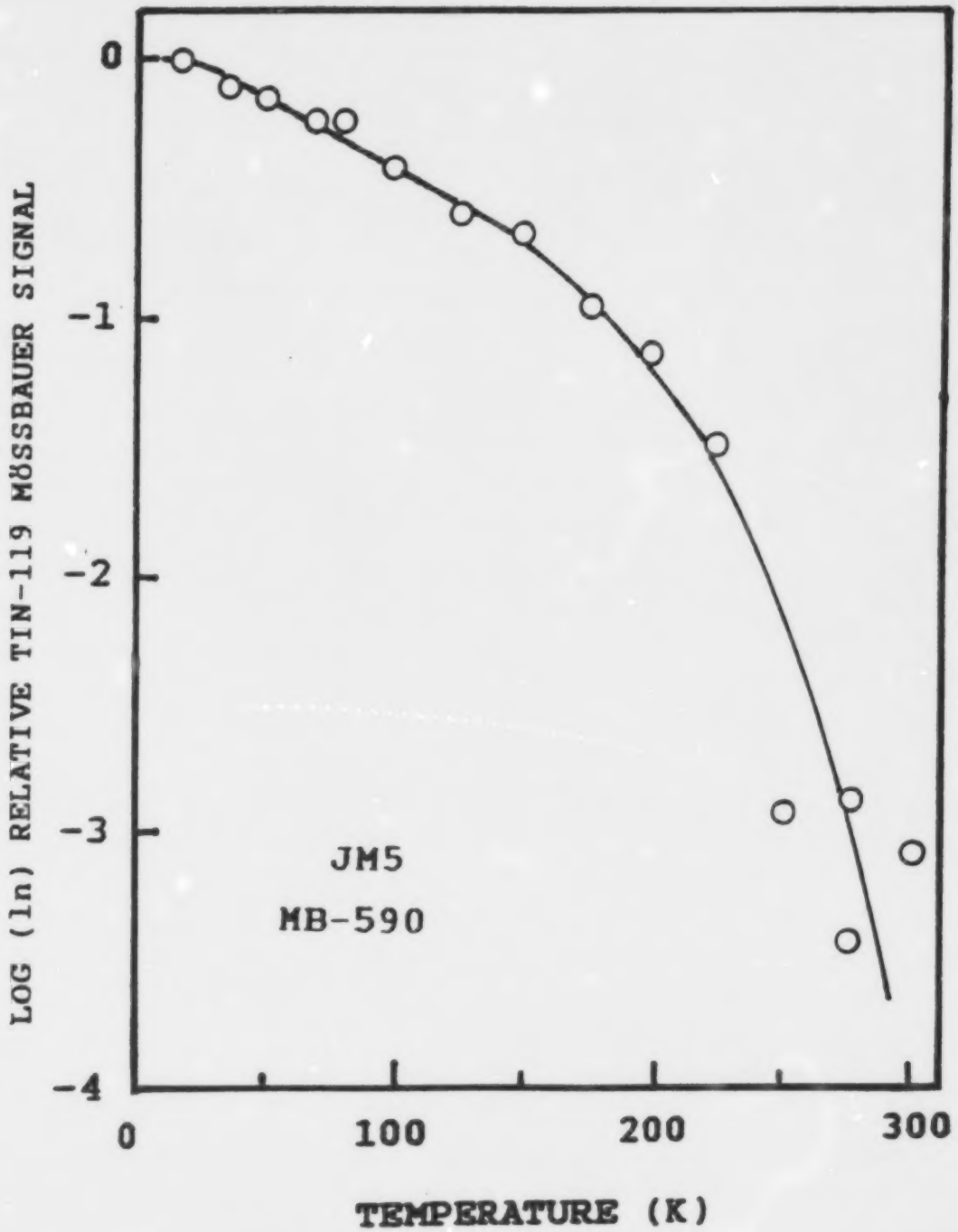

Figure 10: Evolution of the log of the relative intensity of the tin-119 Mössbauer signal versus temperature for Sn/coal (MB-590, JM5).

relative intensity I_R is the ratio of the intensity I_T measured at temperature T to the intensity I_o measured at the lowest temperature, i.e. close to absolute zero. Therefore, the graph of fig. 10, as well as similar graphs for other samples, show:

$$\ln (I_R) = \ln (I_T/I_o) = f(T) \qquad (XX)$$

This graph is the best approximation to the equation below,

$$\ln (f_a) = f(T) \qquad (XXI)$$

which is the desired function, but cannot be obtained unless the exact tin content of the sample is known. In this graph, log (I_R) equals 0 for the lowest temperature since I_T/I_o ---> 1 for T ---> 0. However, as shown by equation XIII, the recoil-free fraction is always smaller than unity, and therefore ln f < 0, even at the zero point motion, since it is equal to the exponential of the inverse of the Debye temperature, which is not infinitely high.

The lattice strength of the Sn(IV)/Cl/O species impregnated in coal is rather low since the zero point motion, with f_a independent of temperature at very low temperature, is not visible, and therefore must be restricted to a narrow temperature range below the capabilities of our refrigeration system (T<15 K). The recoil-free fraction shows a linear decrease with increasing temperature up to ca. 150 K, in agreement with equation XV. Above 150 K, anharmonicity effects take over and become predominent above 230 K. Above 250 K, the Mössbauer signal is extremely weak, and is at the limit of detection at RT. The Debye temperature for this species can be estimated to be close to 300 K.

2.3. Tin catalysts supported on hydrous titanate.

Four tin catalysts supported on hydrous titanates were previously studied in our laboratory (3 and 9-11). Room temperature Mössbauer spectroscopy showed that, although tin, in the divalent state only, was used for their preparation, most of the

tin they contain is tetravalent. Only one sample (JM9) gave a tin(II) signal in ^{119}Sn Mössbauer spectroscopy equal to 25 % of the total Mössbauer spectrum. The others gave a tin(II) signal of 10 % (JM10) or 5 % (JM1 and JM7). However, as discussed above, the low intensity of the tin(II) signal may originate in its recoil-free fraction being lower than that of tin(IV), because of a lower coordination number and less continuity in the bond network because of the stereoactivity of tin(II) lone pair. This can result in a very serious underestimation of the amount of tin(II) in the sample, and an overestimation of the amount of tin(IV). The main purpose of this work was to use low temperature Mössbauer spectroscopy to get a better estimate of the two kinds of tin in the samples. This is possible because the recoil-free fraction of a soft lattice compound increases faster than that of a hard lattice compound, when the temperature is lowered, and the difference between them at very low temperatures is much smaller.

To our big surprise, the Mössbauer spectra recorded at low temperatures, down to 15 K, showed tin(IV) only, with an isomer shift close to zero, indicative of an octahedral or pseudo-octahedral coordination, similar to that found in SnO_2. This was previously also observed before at RT, in addition to the minor divalent tin component coordinated by oxygenated ligands (O, OH and/or H_2O). In order to confirm unambiguously that the divalent tin phase had disappeared from the four non-calcined catalysts, their Mössbauer spectrum was recorded again at ambient temperature in the same conditions as in the previous study. The result was very clear: there was no more divalent tin in the samples. The disappearance of tin(II) can probably be explained by oxidation to tin(IV) by atmospheric oxygen. However, tin(II) oxides such as SnO seem indefinitely stable in air at room temperature. We showed previously (3 and 9-11) that the ion-exchanged non-calcined tin catalysts are highly microcrystalline,

with, as only distinguishable Bragg peaks, extremely broad peaks of stannic oxide SnO_2. No peak for the divalent tin phase was observed, which indicates it is amorphous or microcrystalline with an average particule diameter no larger than ca. 30 Å. Such small particles, maybe present as a thin layer coating the titanate support, may not have the same resistance to oxidative attack by atmospheric oxygen than bulk tin(II) oxide, because of exposure of its high surface area to oxygen molecules present in air. The product of oxidation is microcrystalline stannic oxide. This explains the low amount of tin(II) and high amount of tin(IV) we found previously in the samples. Most likely, oxidation started immediately after preparation and proceeded slowly to completion, which must have occured in the time period of one to three years, depending on the sample, which elapsed from the initial room temperature measurements and the low temperature study. However, the correlation we observed earlier between the amount of tin(II) and the method of preparation (Table XI, in page 72 of ref. 9) is still valid, and initial oxidation of some of the tin(II) in solution must have contributed to the disappearance of tin(II), and resulted in unequal amounts of tin(II) in the four non-calcined catalysts.

The evolution of the relative intensity (equation XX) of the tin(IV) signal with temperature is shown on fig. 11a. In contrast with fig. 10 (note the scale of fig. 11 is expanded), the signal for microcrystalline tin(IV) oxide in the non-calcined catalysts decreases very slowly with increased temperature. The zero point motion is clearly visible, up to ca. 50 K, and the linear region extends to ca. 250 K. A slow acceleration of the decrease of the intensity of the signal, due to anharmonicity of the thermal vibrations, is observed only above 250 K. This is obviously a material with a hard lattice, and its Debye temperature is well above room temperature. This is expected in tetravalent tin oxide.

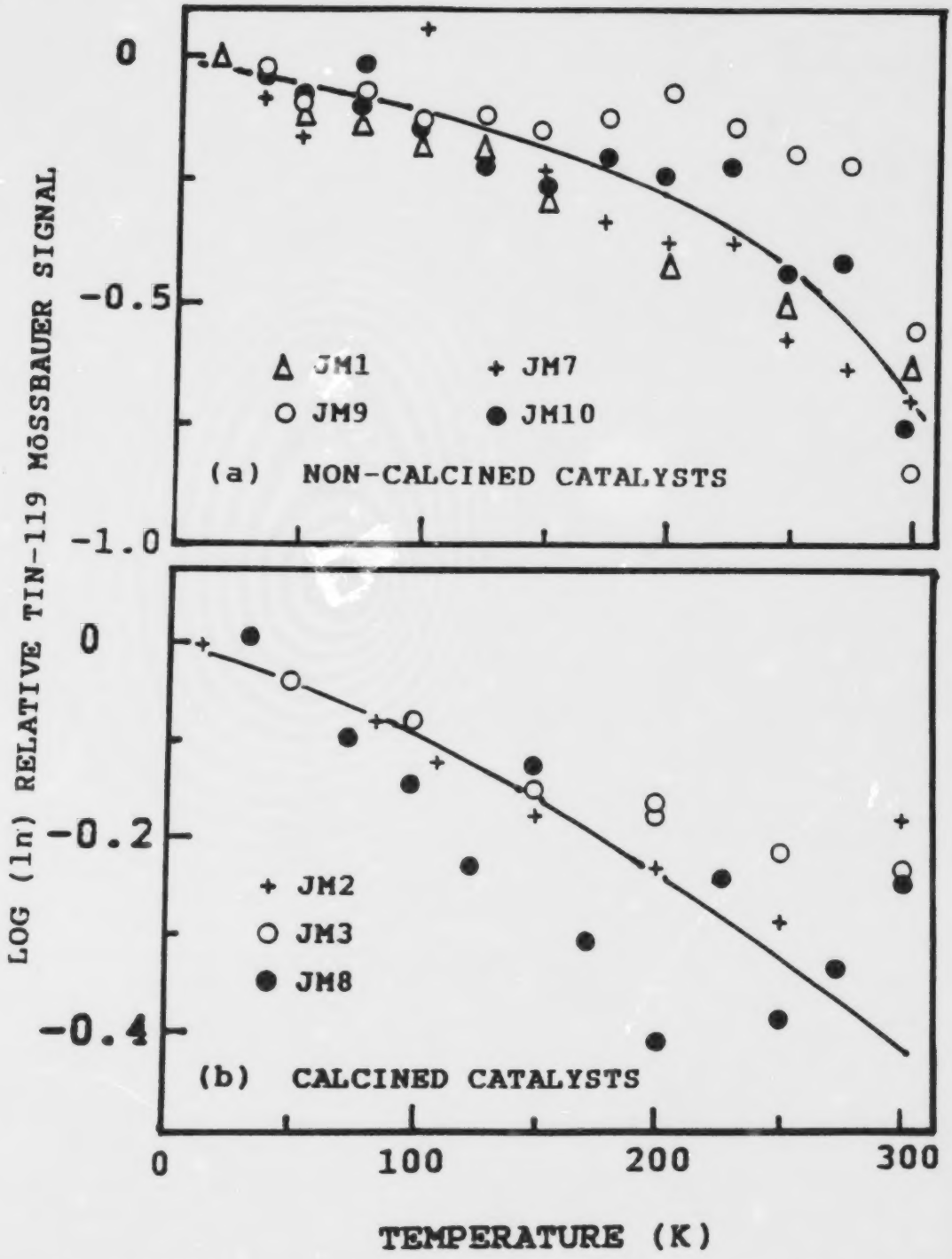

Figure 11: Evolution of the log of the relative intensity of the tin(IV) Mössbauer signal in (a) non-calcined catalysts and (b) calcined catalysts.

3. CALCINED CATALYSTS.

3.1. Introduction.

Four calcined tin catalysts deposited on hydrous titanate (JM2, JM3, JM8 and JM19) were previously studied in our laboratory (3 and 9-11). Electron microscopy showed that not much changes took place on calcination, and the samples were still made of irregular agglomerates of loosely bound particles with no internal structure. The absence of texture was in good agreement with X-ray diffraction results which showed that, although the crystallites were bigger (up to ca. 300 Å), this minor crystallite growth could not be observed by our electron microscope, the samples were still microcrystalline and no sintering occured. Depending on the sample, some of the following oxides, in the microcrystalline state, were identified after calcination: TiO_2 anatase, TiO_2 rutile, SnO_2 rutile and a rutile type $Ti_{1-x}Sn_xO_2$ solid solution. Mössbauer spectroscopy at ambient temperature showed that only tin(IV) octahedrally or pseudo-octahedrally coordinated by oxygen was present. This type of tin, similar to the tin(IV) observed in the non-calcined catalysts, present a coordination similar to that found in SnO_2. No signal for divalent tin was detected. As expected, heating at 400 °C in air for two hours resulted in the oxidation of the tin(II) present before calcination to tin(IV).

In addition to the tin catalysts, we were provided with three new samples, cobalt/molybdenum catalysts deposited on titanates, calcined at 150, 350 and 500 °C, respectively. These were not studied earlier by us. In this work, they were characterized by electron microscopy and X-ray powder diffraction.

3.2. Calcined tin titanate catalysts.

Low temperature Mössbauer spectroscopy gives a single peak, for SnO_2 type tin(IV), in the range 15-300 K. No peak for divalent tin was observed even at the lowest temperatures. This

is not surprising since tin(II) could not have survived calcination in air at 400 °C. The evolution of the relative tin Mössbauer signal, as defined in equation XX, as a function of temperature, is given on fig. 11b. The behavior is quite similar to that of non-calcined catalysts (fig. 11a), i.e. a very gentle decrease of the signal as temperature is raised. However, the Debye temperature for the calcined catalysts is even higher than for the non-calcined ones, since the linear region extends to RT, and heating above ambient temperature would be required in order to detect anharmonicity effects. This is not surprising, since after calcination, the anhydrous oxides most likely contain only bridging oxygen as metal ligands, and therefore results in a very strong three-dimensional lattice. On the other hand, before calcination, some of the water molecules may be located in the first sphere of coordination of tin(IV), as terminal H_2O molecules or hydroxyl anions. This would result in a small weakening of the overall lattice strength at tin, and hence a slightly lower recoil-free fraction. However, since the difference should be small, one would not expect to detect it at low temperature where the amplitude of the thermal vibrations of these strong lattices is small. To the contrary, at high temperatures, far away from the zero point motion, the difference should increase with temperature. Indeed, this is observed, and at room temperature, the signal loss is twice as high in the non-calcined sample, as can be seen on fig. 11 (caution: the vertical scale of fig.11b is much more expended than that of fig.11a, which also amplifies the dispersion of the experimental points on the graph).

3.3. Calcined cobalt-molybdenum titanate catalysts.

3.3.1. Scanning electron microscopy.

The three samples (MB-592) received from CANMET were examined by Scanning Electron Microscopy (SEM) at the maginifications of 100, 500 and 2000. The following results were obtained:

3.3.1.1. Sample #64 (JM23): MB-592 (150 °C).

x100 (fig. 12): Irregular particles of all kinds of shapes and sizes are observed, some as large as 150 - 200 μm diameter, but most are in the range 20 - 100 μm. These large particles appear covered with a dust of much smaller particles.

x500 (fig. 13): Some of the big particles seem to be platelets, with a fairly smooth surface, and partly covered with very small particles while others seem to be just bulkier agglomerates of small particles.

x2000 fig. 14): These pictures confirm the polycrystalline nature of the big particles. The small particles which are located on the surface of the big particles have a dimension smaller than 1 μm, and probably are as small as 1,000 Å or even less. A plate 6 μm thick and of 43 μm edge is clearly visible on one of the photographs. The thickness is not regular and a large part is chipped off a corner. Smaller particles are located on the surface of the plate.

3.3.1.2. Sample #65 (JM24): MB-592 (350 °C).

x100 (fig. 15): Irregular particles of about the same size as for JM23 are observed.

x500 (fig. 16): The big particles seem to be agglomerates of much finer particles. No platelets are observed as these agglomerates look bulkier.

x2000 (fig. 17): This picture confirms the polycrystallinity and agglomerate nature of the material and the absence of plates.

3.3.1.3. Sample #66 (JM25): MB-592 (500 °C).

x100 (fig. 18): The particles are smaller than for the two previous samples. A few are as large as ca. 100 μm edge but most are in the range 20-50 μm or smaller.

x500 (fig. 19): These pictures confirm the more fragmented nature of the particles. Some smaller platelets covered with powder are observed.

x2000 (20): The particles seem much more divided than for the previous samples. They are made of very small particles (probably less than 1000 Å diameter) which form less compact agglomerates.

Figure 12: SEM x100 of JM23: MB-592 calcined at 150 °C

Figure 13 (a): SEM x500 of JM23: MB-592 calcined at 150 °C

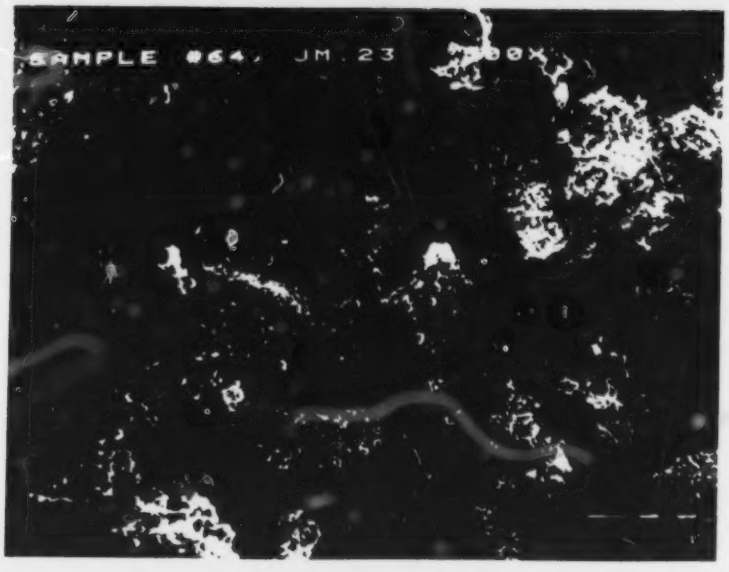

Figure 13 (b): SEM x500 of JM23: MB-592 calcined at 150 °C

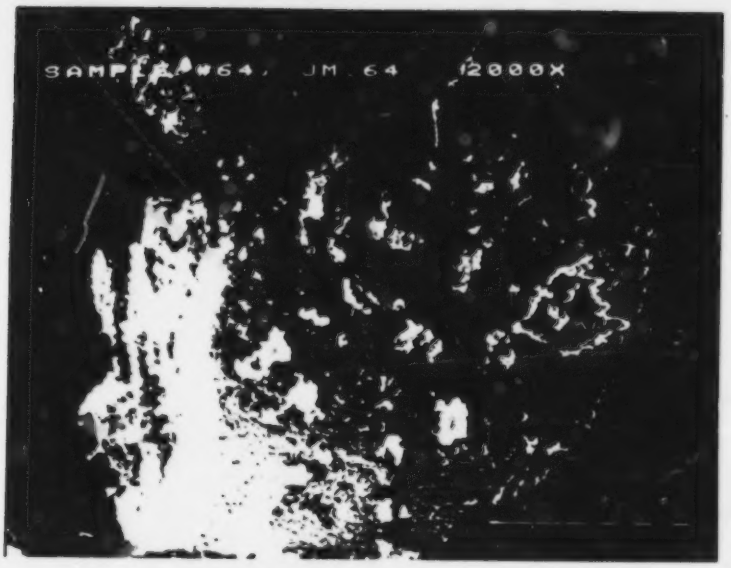

Figure 14 (a): SEM x2000 of JM23: MB-592 calcined at 150 °C

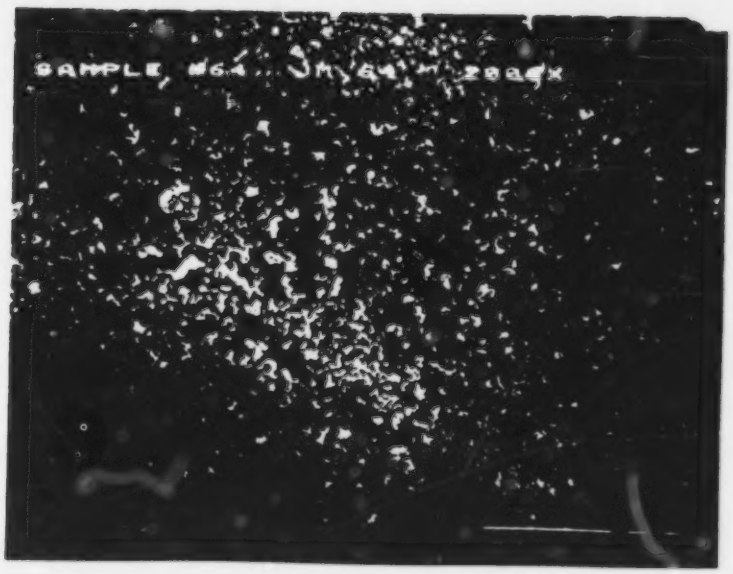

Figure 14 (b): SEM x2000 of JM23: MB-592 calcined at 150 °C

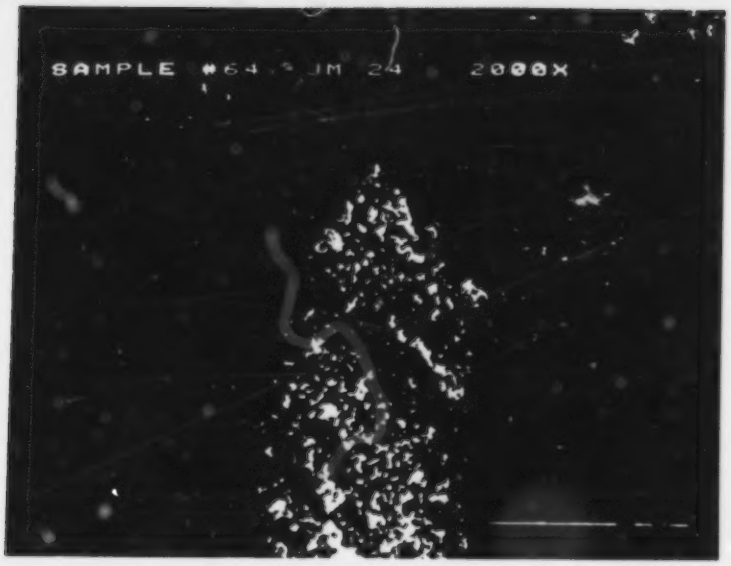

Figure 14 (c): SEM x2000 of JM23: MB-592 calcined at 150 °C

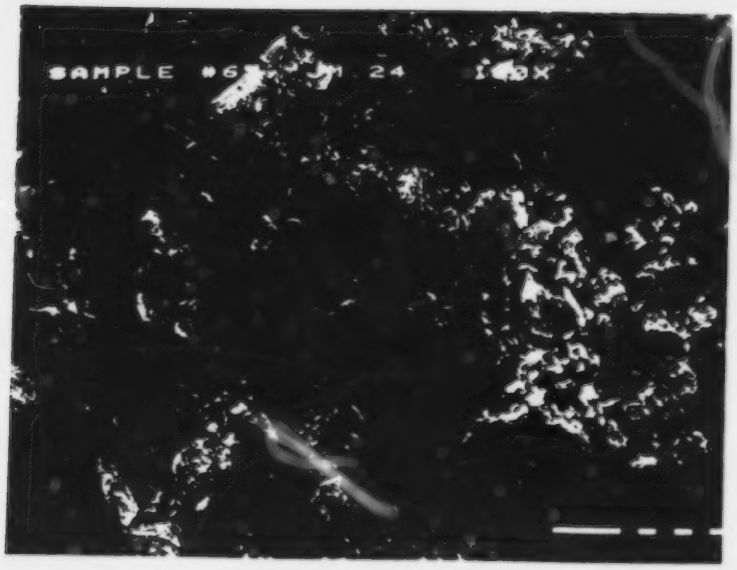

Figure 15: SEM x100 of JM24: MB-592 calcined at 350 °C

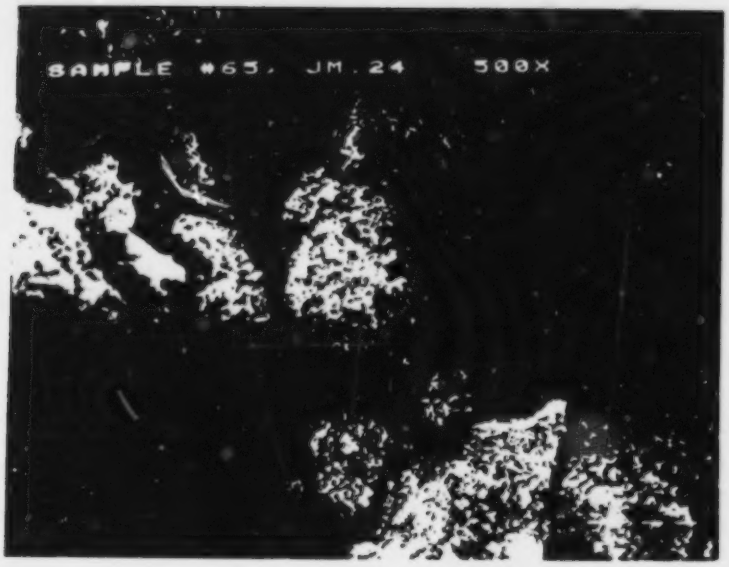

Fig. 16 (a): SEM x500 of JM24: MB-592 calcined at 350 °C

Fig. 16 (b): SEM x500 of JM24: MB-592 calcined at 350 °C

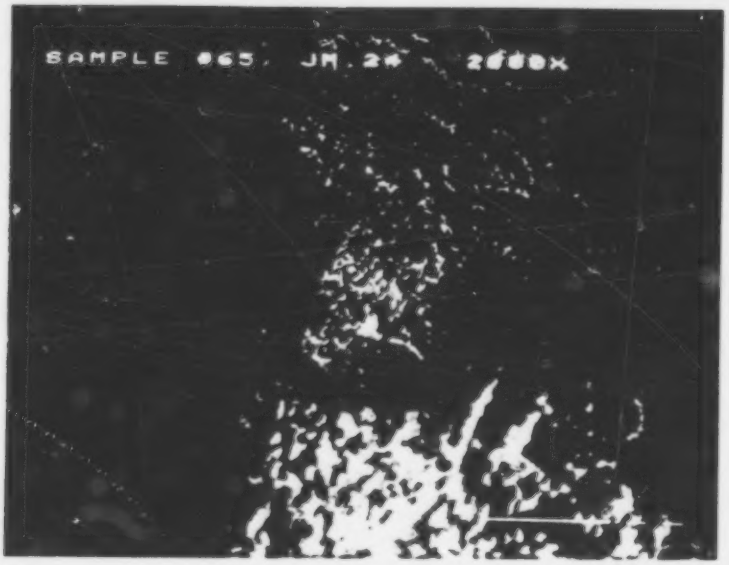

Figure 17: SEM x2000 of JM24: MB-592 calcined at 350 °C

Figura 18: SEM x100 of JM25: MB-592 calcined at 500 °C

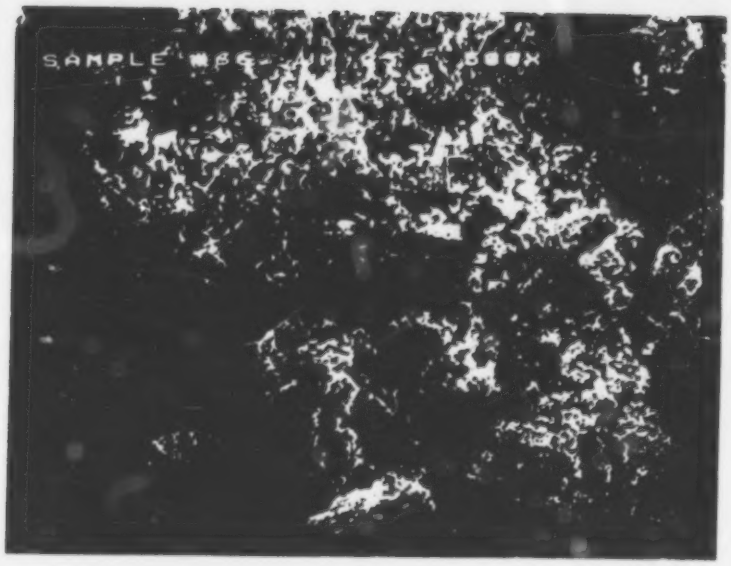

Figure 19 (a): SEM x500 of JM25: MB-592 calcined at 500 °C

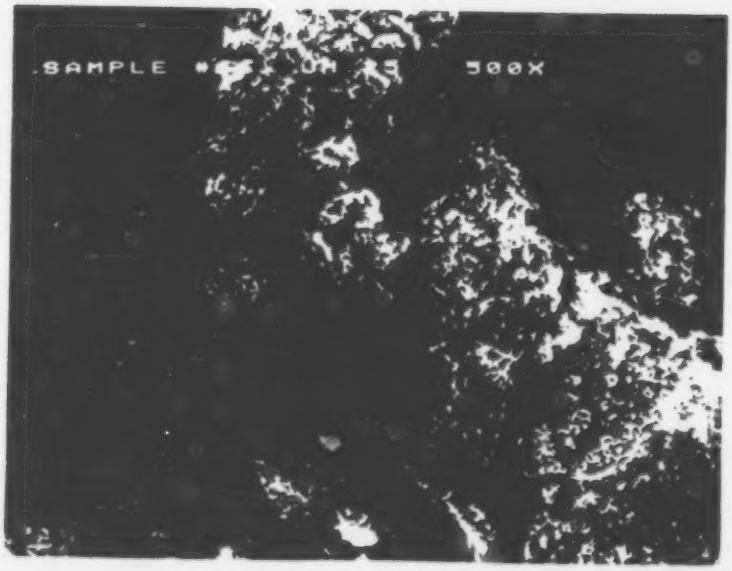

Figure 19 (b): SEM x500 of JM25: MB-592 calcined at 500 °C

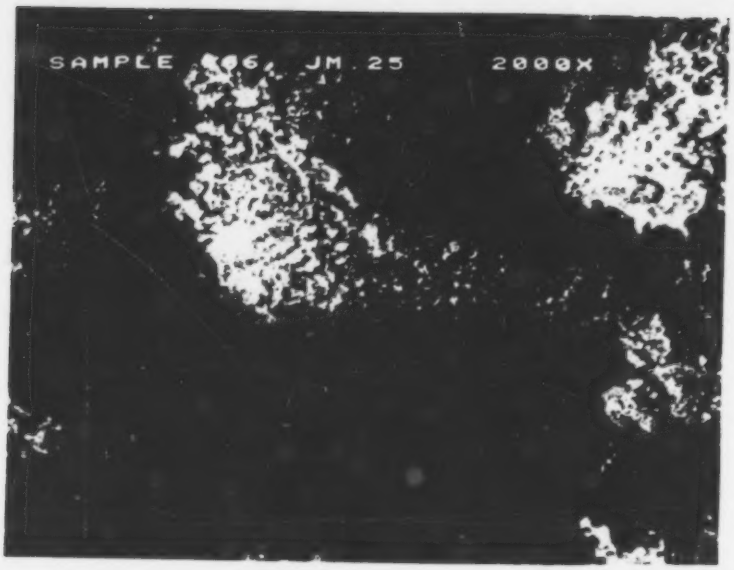

Figure 20 (a): SEM x2000 of JM25: MB-592 calcined at 500 °C

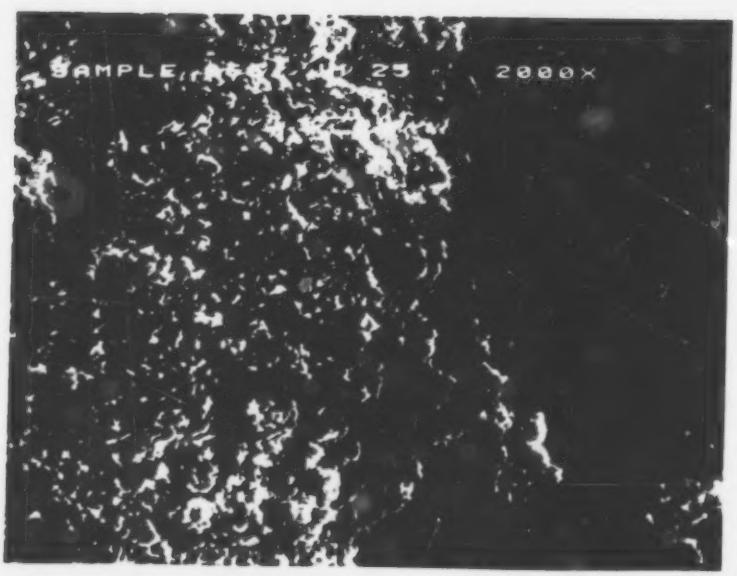

Figure 20 (b): SEM x2000 of JM25: MB-592 calcined at 500 °C

3.3.2. X-ray powder diffraction.

The X-ray powder pattern for the three MB-592 samples show their poor crystallinity (fig. 21) and corroborates our observations using electron microscopy. The samples calcined at 150 °C (JM23) and 350 °C (JM24) show no Bragg peak at all, and therefore are amorphous or microcrystalline with a particle size not larger than ca. 30 Å. On the other hand, after calcination at 500 °C, some broad diffraction peaks are observed. Since the support of the Co-Mo catalysts was hydrous titanate, and TiO_2 anatase was previously found (3 & 9-11) to be the main crystalline component of the tin catalysts JM2, JM3 and JM8 supported on hydrous titanate, it seemed appropriate to us to compare the X-ray powder patterns of MB-592 calcined at 500 °C (JM25) with that of commercial TiO_2 anatase. Examination of the two powder patterns (fig. 21) clearly shows that microcrystalline anatase (peaks unlabelled) was formed and is the major crystalline component of the catalyst.

The broadening of the (101) peak of anatase in JM25 was used, in reference to the linewidth of the same peak for commercial anatase (which has unbroadened lines), to calculate the average particle size of anatase in the catalysts calcined at 500 °C. The average particle diameter t(Å) was calculated using Scherrer's formula (33):

$$t = (0.9*\lambda)/(B*\cos\theta) \qquad \text{(XXII)}$$

where t is the average particle diameter in Å,
λ is the wavelength of the radiation in Å,
θ is the Bragg angle for the Bragg peak used, and
B is the broadening at half height (in radians) due to the small dimension of the particles.

Correction for instrumental line broadening was performed using Warren's method (33):

$$B^2 = B_M^2 - B_s^2 \qquad \text{(XXIII)}$$

where B_M is the experimental linewidth for the sample (in

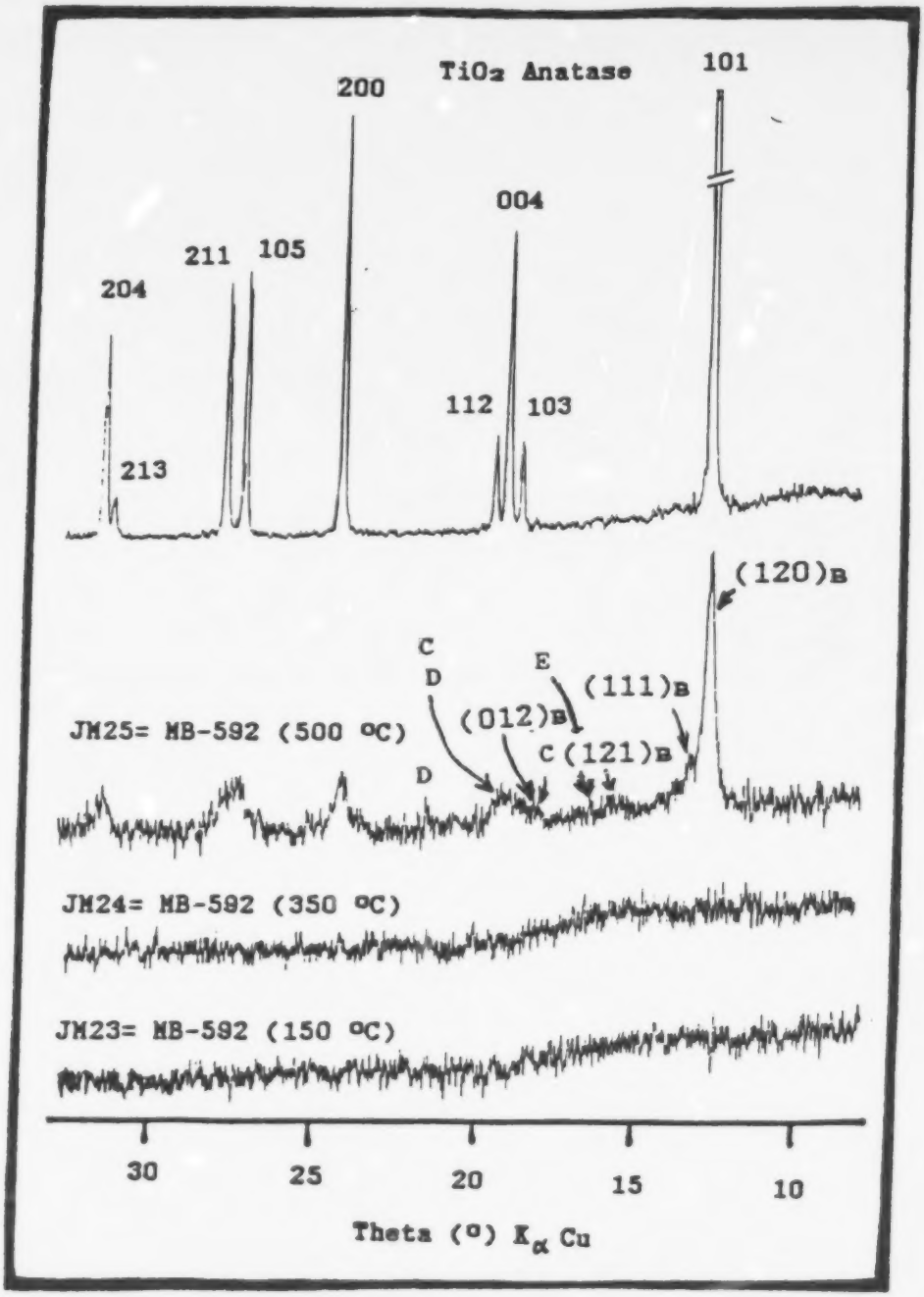

Figure 21: X-ray powder diffraction patterns of MB-592 Co-Mo catalyst deposited on hydrous titanate, after calcination at 150 °C, 350 °C and 500 °C, respectively. The powder pattern of TiO_2 anatase is given for comparison. For JM25 = MB-592 (500 °C), the peaks are labelled according to the following code: unlabelled= TiO_2 anatase, $(hkl)_B$= $CoMoO_4$, C= $Co_3Mo_3O_8$, D= CoO and E= Co_3O_4.

radians)

B_s is the experimental linewidth for a well crystalline standard material.

A material with a particle size larger than 1,000 Å gives no line broadening due to particle size, and therefore can be used as a standard. Commercial TiO_2 anatase gave a linewidth of 0.17 ° (θ); this is the same as we usually obtain in the same angular region for well crystalline materials using our equipment, therefore anatase was used here for standard of instrumental broadening. The experimental linewidth for the (101) peak of anatase in the catalyst was 0.38 ° (θ), and calculation gave an average particle diameter of 240 Å. This compares well to the values of 301 Å (JM1), 330 Å (JM3) and 139 Å we found previously in calcined tin catalysts on hydrous titanate (3 & 9-11).

In addition to TiO_2 anatase, a few other weaker broad peaks can be seen on the powder pattern of JM25 (fig. 21). We considered that any known combination of the oxides of titanium, cobalt and/or molybdenum may be formed in the microcrystalline state and be responsible for the extra Bragg peaks. This was checked using the JCPDS Powder Diffraction File (32). The results are summarized in Table VIII. $CoMoO_4$, in the phase described in the JCPDS file No. 21-868 (32) is most likely present in the catalyst. Other phases that may be present in smaller quantities are $Co_2Mo_3O_8$, CoO and Co_3O_4, however, their presence is difficult to ascertain because of the microcrystallinity of the sample and the overlap of the strongest peaks of the above compounds with the strongrest peaks of TiO_2 anatase. These results can be compared to the study of the surface of the catalyst by Monnier et al. (4) using X-ray photoelectron spectroscopy (XPS). The XPS study indicates the probable presence of $CoMoO_4$, $CoTiO_3$ or $Co(OH)_2$ in the sample. X-ray diffraction allows a more specific identification of the phases present, since it clearly shows that $CoMoO_4$ is

Table VIII: Results of the search for mixed oxides of Ti, Co and/or Mo in JM25, using the JCPDS Powder Diffraction File (32).

Compound	JCPDS File	Presence in the catalyst	Label of peaks on figure 21	XPS Results (ref. 4)*
TiO_2 anatase		Yes	Unlabelled	-
$CoMoO_4$	21-868	Most likely	$(hkl)_m$	Most likely
$CoMoO_4$	25-1434	No	-	-
$CoMoO_4$	16-309	No	-	-
$CoMoO_3$	21-869	No	-	-
$Co_2Mo_3O_8$	34-511	Possible	C	-
$CoTi_2O_5$	35-793	Probably not	-	-
$CoTiO_3$	15-866	No	-	Most likely
$CoTiO_3$	29-516	No	-	-
Co_2TiO_4	18-428	No	-	-
α-$Co(OH)_2$	2-925	No	-	Most likely
β-$Co(OH)_2$	30-443	No	-	-
CoO	9-402	Possible	D	No
Co_3O_4	9-418	Possible	E	No

*The XPS results of (4) do not specify which phase of $CoMoO_4$, $CoTiO_3$ or $Co(OH)_2$ is most likely to be present. In addition, one of the three compounds $CoMoO_4$, $CoTiO_3$ or $Co(OH)_2$, not the three of them, is said to be most likely present.

present, whereas $CoTiO_3$ and $Co(OH)_2$ are not. In addition to XPS, X-ray diffraction also specifies which phase of $CoMoO_4$ is present. The difference between the two techniques lies in the fact that XPS identifies species present by a shift of emission peaks (chemical shift due to bonding, mostly in the first sphere of coordination of the element being probed) , whereas X-ray powder diffraction checks for the presence of a specific set of diffraction peaks. In X-ray diffraction, each peak is called a "Bragg peak" because its position is determined by "Bragg's law", and the the whole set of Bragg peaks of a given crystalline phase is called its "powder pattern". Since several species may have very close line shifts in XPS, especially when the first sphere of coordination of the element of interest is very similar in several compounds, unambiguous identification may not be possi-

ble. On the other hand, not two crystalline compouds have the same X-ray powder pattern, with the exception of isostructural compounds, and even in this case a line shift also exists due to difference in the size of the unit-cell, therefore, X-ray powder diffraction usually allows a completely unambiguous identification of the crystalline phase present, and even of the specific phase for polymorphic compounds, since polymorphs have different crystal structures (even though their chemical formula is the same), and hence, a different X-ray powder pattern. However, the drawback of diffraction techniques is that they are limited to crystalline phases. Microcrystalline compounds give less accurate results, depending on the degree of crystallinity and the complexity of the mixture, and amorphous phases are undetectable. On the other hand, XPS is a local probe and therefore can also detect non-crystalline phases. Therefore, XPS could have measured amorphous phases in the catalyst, that would not be detected by X-ray diffraction, however, examination of Table VIII shows that none was found. Another difference between the results obtained by the two methods is that CoO or Co_3O_4 are ruled out by XPS, whereas X-ray diffraction shows they may be present. This is not contradictory since XPS probes the surface of the solid (electrons cannot escape from solids unless they are ejected within ~ 20 to 50 Å from the surface) whereas X-rays in the range of wavelengths most commonly used for diffraction (0.5 - 2 Å) penetrate solids to a depths of several tens or several hundreds of micrometers, i.e. at least 10^3 to 10^4 deeper than in electron spectroscopies. Therefore, the amount of material probed by XPS is only in the order of magnitude of 0.1 to 0.01% of that probed in X-ray diffraction. It results that XPS probes the surface of solids, whereas X-ray diffraction probes the bulk, and the surface contributes too little to the X-ray diffraction pattern to be detected. Therefore, combined XPS and X-ray diffraction show that $CoMoO_4$ is present in both the surface and the bulk. In addition, $Co_2Mo_3O_8$ may be present in the bulk; in

addition, CoO and Co_3O_4 may also be present in the bulk, but not on the surface. The reader can find more details on the characterization of solids by electron spectroscopies in ref. 34, and on X-ray diffraction in ref. 33 & 34.

4. USED CATALYSTS.

4.1. Introduction.

Four catalysts supported on hydrous titanates were previously characterized in our laboratory using the techniques of X-ray powder diffraction and room temperature Mössbauer spectroscopy (3 & 9-11). The samples were JM4 (test # 54), JM6 (test # 55), JM11 (test # 63) and JM12 (test # 76). It was found that the samples were still microcrystalline after hydroprocessing tests, therefore, no further crystal growth or sintering had occured on heating at 410 °C under reducing conditions. The main change was the formation of SnS in variable quantities. Reduction of tin(IV) to tin(II) in the coal/hydrogen reducing medium occured, together with sulfidation of the tin(II) that was formed. Coal, and to a lesser extent, oil, are the sources of sulfur. The two reactions (reduction of tin and sulfidation) are probably combined in an overall process, since no tin(II) oxide was found, unless sulfidation is faster than reduction, which would make the overall kinetics of the process dependent on the slowest reaction step, i.e. reduction. Mössbauer spectroscopy at ambient temperature showed that significant amounts of SnS were obtained only if the catalyst used was made of the rutile type $Ti_{1-x}Sn_xO_2$ (MB-599 ---> JM11 and JM12). In addition, TiO_2 anatase, which was not present in the unused catalyst, was formed during the hydroprocessing test. These findings lead to the conclusion that the rutile type $Ti_{1-x}Sn_xO_2$ solid solution is decomposed during the test to give TiO_2 anatase and at the same time, the tin(IV) released is reduced by hydrogen and carbon and

sulfided to SnS. This conclusion is reinforced by the fact that the catalysts that did not contain the rutile type solid solution, i.e. MB-586 and MB-587, show no more than 1 % of the total tin in the form of SnS after the hydroprocessing test. Even for JM4, which contained a significant amount of SnO_2 rutile before the test, only 1 % SnS was observed after testing. This showed that SnO_2 rutile is not reduced like the Sn(IV) from the solid solution of same structure, during hydroprocessing.

We were provided for this project with four additional used catalysts:
(i) Test # 52 (JM31): used tin supported on coal (MB-590);
(ii) Test # 115 (JM20 and JM26): used tin supported on coal (MB-590);
(iii) Test # 116 (JM21 and JM27): used tin supported on coal (MB-590);
(iv) Test # 123 (JM22 and JM28): used tin supported on hydrous titanate (MB-599).
Contrary to all other used catalysts, the catalysts used in the tests # 115, 116 and 123 were supplied mixed with heavy hydrocarbons (before washing with THF). The reason for this is explained in the appropriate paragraph below.

4.2. <u>Tin-119 Mössbauer spectroscopy at ambient temperature</u>.

The Mössbauer spectroscopic results at RT for JM20, JM21, JM22, JM26, JM27, JM28 and JM31 are compared in Table IX to those of the other used catalysts (i.e. JM4, JM6, JM11 and JM12) studied previously (3 & 9-11) and to literature about SnO_2 and SnS. Clearly, there are three kinds of catalysts, in terms of amount of SnS produced in the hydroprocessing reaction:
(i) No SnS produced (JM4 & JM6): As outlined above, no (or very little) SnS is produced in the hydroprocessing test when tin(IV) is present in the form of SnO_2 rutile. This is probably due to the low reactivity of SnO_2, which seems to escape reduction under

Table IX: Mössbauer spectroscopic results at ambient temperature for the used catalysts.

Sample	Catalyst	Species	δ(mm/s)	Δ(mm/s)	% signal
JM4	MB-586	Sn(IV)	-0.03	0.40	99
		SnS	3.16	0.98	1
JM6	MB-587	Sn(IV)	-0.03	0.00	>99
JM11	MB-599	Sn(IV)	-0.03	0.00	85
		SnS	3.22	0.86	15
JM12	MB-599	Sn(IV)	-0.03	0.00	90
		SnS	3.28	0.86	10
JM20	MB-590	Sn(IV)	-0.06	0.00	27
		SnS	3.24	0.79	73
JM21	MB-590	Sn(IV)	0.00	0.00	22
		SnS	3.17	0.76	78
JM22	MB-599	Sn(IV)	-0.06	0.00	82
		SnS	3.14	0.82	18
JM26	MB-590	Sn(IV)	-0.08	0.00	34
		SnS	3.34	0.76	66
JM27	MB-590	Sn(IV)	0.00	0.00	24
		SnS	3.34	0.76	76
JM28	MB-599	Sn(IV)	-0.07	0.00	85
			3.31	0.84	15
JM31	MB-590	Sn(IV)	0.00	0.00	30
		SnS	3.16	0.70	70
SnO_2	Ref. 35	Sn(IV)	0.00	0.64	100
SnS	Ref. 36	SnS	3.29	0.87	100

Notes:

1. δ = isomer shift ($\pm$0.01), relative to $CaSnO_3$ at RT.
2. Δ = quadrupole splitting ($\pm$0.01).

the conditions of the tests.

(ii) 10 to 20 % SnS produced (JM11, JM12 & JM28): We found previously (3 & 9-11) that the used catalysts JM11 and JM12 contained 10 to 15 % of SnS, and that simultaneously, TiO_2 anatase, not present in the MB-599 catalyst before the test, had formed during the test, and at the time, the amount of rutile type $Ti_{1-x}Sn_xO_2$ had decreased. This was attributed to the decomposition of the solid solution, with liberation of TiO_2, which crystallizes in its most stable form, i.e. anatase, and with liberation of and "activated" SnO_2 which is reduced by hydrogen and carbon to Sn(II), instead of crystallizing to its stable and highly unreactive rutile form. Then, the divalent tin formed is sulfided to SnS by the sulfur contained in coal. These results are corroborated by the samples JM22 and JM28 (test # 123 on calcined MB-599 catalyst), which we found to contain 18 and 15 % of SnS, respectively.

(iii) 65 to 80 % SnS produced (JM20, JM21, JM26, JM27 and JM31): All these used catalysts originate from tin supported on coal MB-590 (JM5). The much larger amount of SnS formed is striking. This can certainly be attributed to the strength of the Sn-Cl bonds, which is much smaller than that of the Sn-O bonds, as shown by low temperature Mössbauer spectroscopy: from the data of fig. 10 and 11b, one can easily calculate that the intensity of the tin-119 Mössbauer signal for Sn supported on coal (JM5= MB-590) at RT is only ca. 2 % of the intensity measured at 15 K (fig.10). This strongly contrasts with the calcined tin catalysts supported on hydrous titanate, which still give a signal equal to about 67 % of its value at 15 K. Comparing these results to fig.4, shows unambigously that the tin(IV) oxide in the calcined catalysts has a very strong lattice, whereas the tin(IV) oxicloride supported on coal has a much softer lattice. The much larger amount of SnS formed using the tin(IV) oxichloride supported on coal catalyst is in agreement with the total disappearance of the peak at δ = 0.36 mm/s (Table VII) and the

appearance of a tin(IV) oxide peak at $\delta \sim 0$ mm/s (Table (IX) during the hydroprocessing test. It seems strange that tin(IV) oxide could be formed in the highly reducing medium (hydrogen under pressure + coal) of the hydroprocessing test. However, the isomer shift of JM5 (Table VII) indicates that, in addition of chlorine, some oxygen ligands are also coordinating tin(IV). This is most likely the oxygen which is used to form tin(IV) oxide, and it indicates once more the strength of the tin(IV)-oxygen bonds.

Another aspect of the characterization of used tin catalysts by Mössbauer spectroscopy at RT is the study of the effect of homogeneization of the mixture catalyst, solid residues and heavy hydrocarbons on the Sn(II)/total Sn ratio in the used catalysts. At the end of the hydroprocessing tests, the liquids were drained and the solids were washed with THF to remove all the heavy hydrocarbons. In the process of separating the heavy hydrocarbons from the solid residues, which contain the used catalyst, unreacted coal, and coke which is formed as an undesirable by-product in some reactions, the viscosity of the mixture is reduced by gentle heating. There was some concern that divalent tin compounds, which are known to oxidize readily when heated, could be oxidized when the mixture is warmed up in order to homogeneize it. This was checked by recording the tin-119 Mössbauer spectrum of the mixture not separated from the heavy hydrocarbons, before and after homogeneization. Examination of fig. 1 and Table IX shows that, although a decrease of the relative amount of SnS occured in all the three samples examined, the change was minor, and to our view, not indicative of any significant degree of oxidation:

- run # 115: JM20 (73 % SnS) ----> JM26 (66 % SnS);
- run # 116: JM21 (78 % SnS) ----> JM27 (76 % SnS);
- run # 123: JM22 (18 % SnS) ----> JM28 (15 % SnS).

This is not surprising since the large excess of heavy hydrocar-

bons coats the catalyst residue with a thick protective layer, which prevents exposure of divalent tin to atmospheric oxygen. Only on the top surface of the mixture, one could envisage short possible exposure to the atmosphere, and even this should be minor, as corroborated by our Mössbauer spectroscopic measurements before and after homogeneization.

4.3. Tin-119 Mössbauer spectroscopy at low temperature.

The Mössbauer spectra of three of the used catalysts (JM4, JM11 and JM12) was investigated as a function of temperature in the range 15-300 K, in the same conditions than for the non-calcined and the calcined catalysts, as reported above. For JM12, the temperature range 150-275 K could not be studied because the heating element on the tip of the cooling system broke down and the replacement part has not be delivered yet. However, the data for 15-125 K and for RT are sufficient to show the effect of temperature and lattice strength on the intensity of the relative Mössbauer signal for SnS and tin(IV) oxide.

The results are presented on fig. 22-28. The general behavior of the three samples is the same. The main feature is the fast decrease of the intensity of the SnS, compared to the hard lattice tin(IV) oxide species. This is evidenced by the graphs of the relative tin-119 signals (fig. 24 & 27) for the two tin containing species, by the graphs of the log of their relative signals (fig. 22, & 25), and by the graphs of the ratio SnS/Total tin (fig. 23, 26 & 28). The graphs of the log follow the theoretical model of the Debye theory (fig. 4) within experimental error. It is obvious from these results that the SnS lattice is much softer than that of Sn(IV) oxide, as expected, and ignoring this effect on their recoil-free fraction at room temperature would result in a gross underestimation of the relative amount of SnS in the sample. The behavior of JM11 was found to be somewhat different at low temperatures, since we

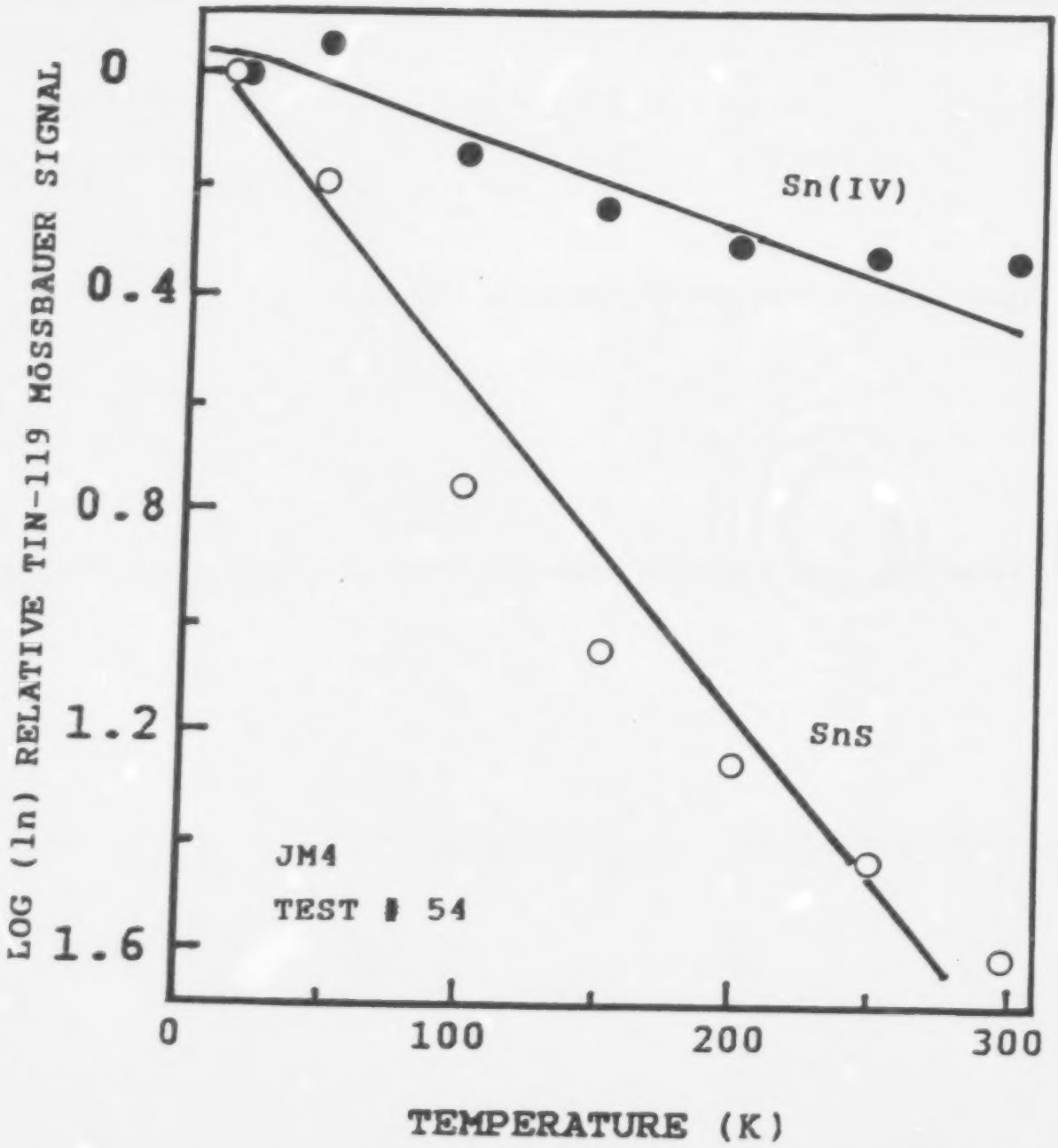

Figure 22: Evolution of the log of the relative intensity of the tin(IV) Mössbauer signal and of SnS in JM4 used catalyst.

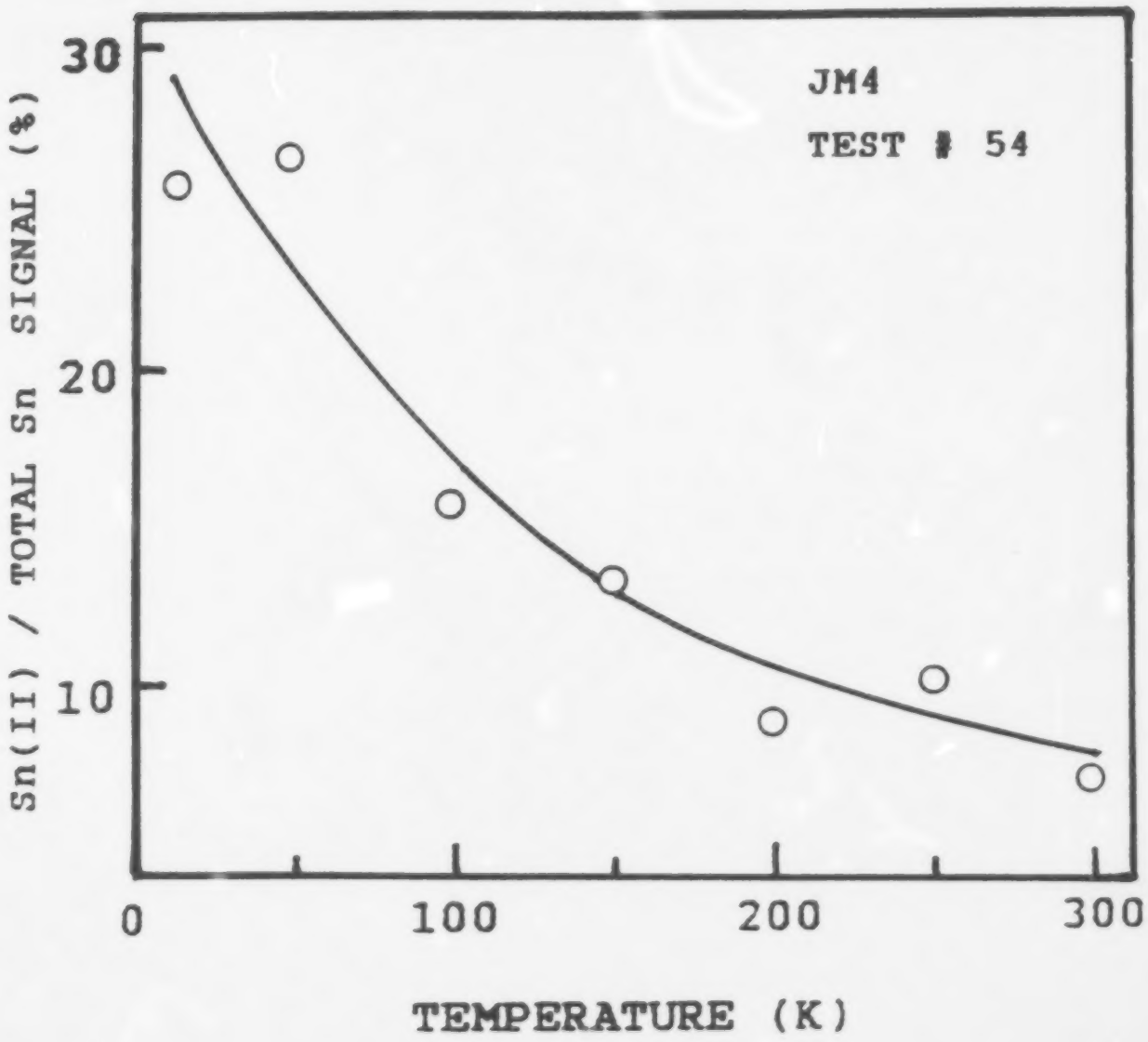

Figure 23: Ratio SnS/Total tin Mössbauer signal versus temperature for JM4 used catalyst.

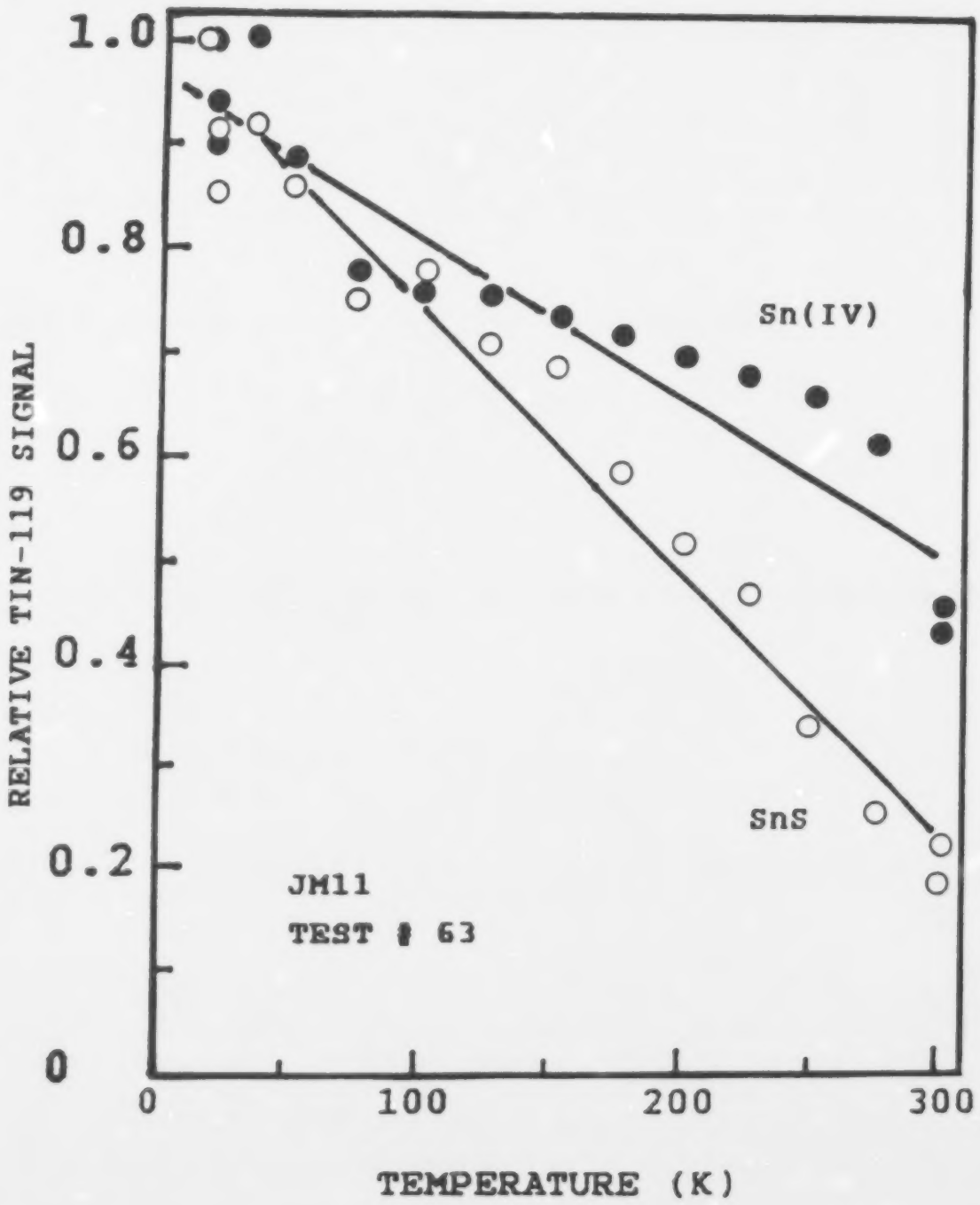

Figura 24: Relative tin-119 Mössbauer signal versus temperature for JM11 used catalyst.

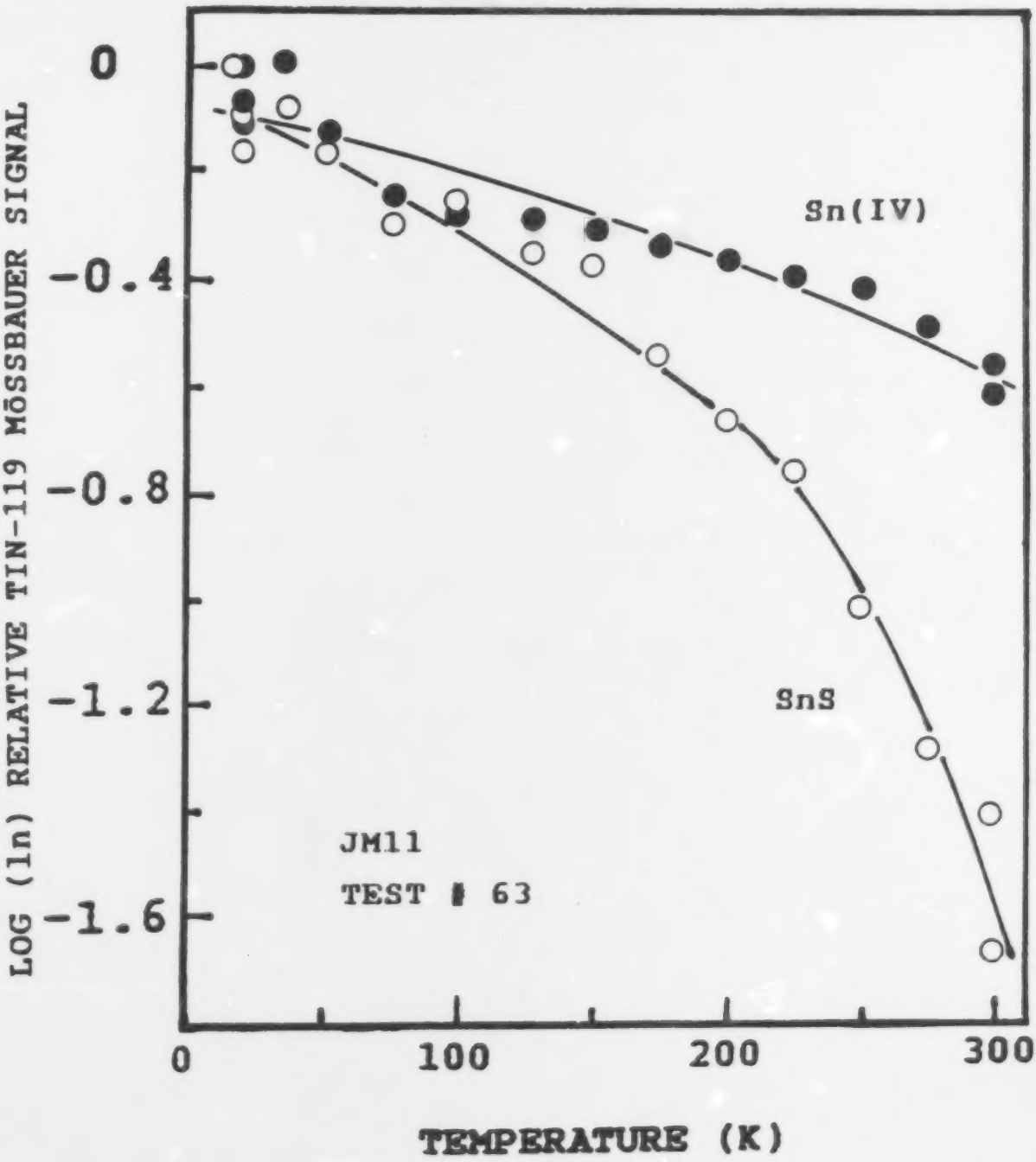

Figure 25: Evolution of the log of the relative intensity of the tin(IV) Mössbauer signal and of SnS in JM11 used catalyst.

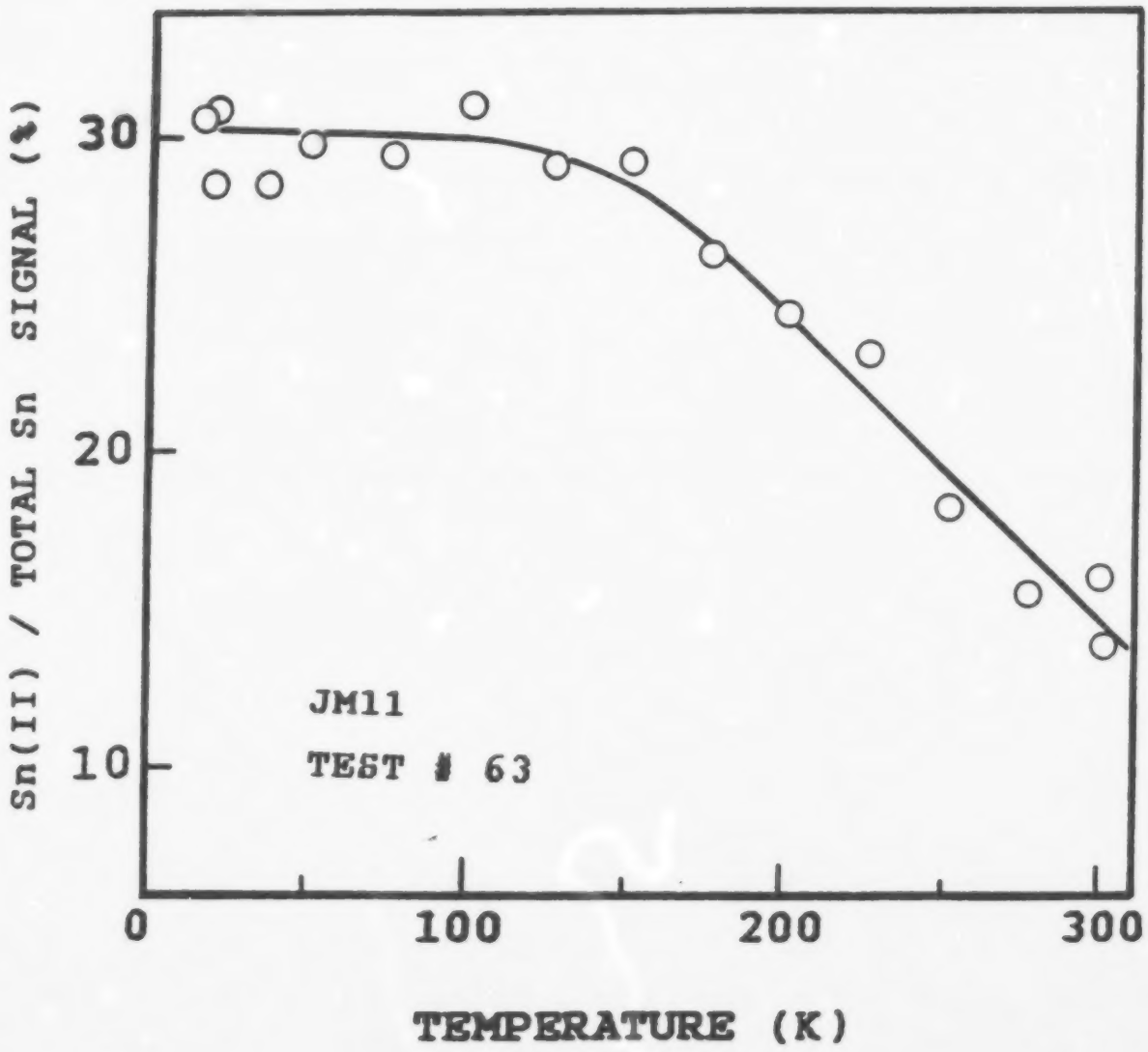

Figure 26: Ratio SnS/Total tin Mössbauer signal versus temperature for JM11 used catalyst.

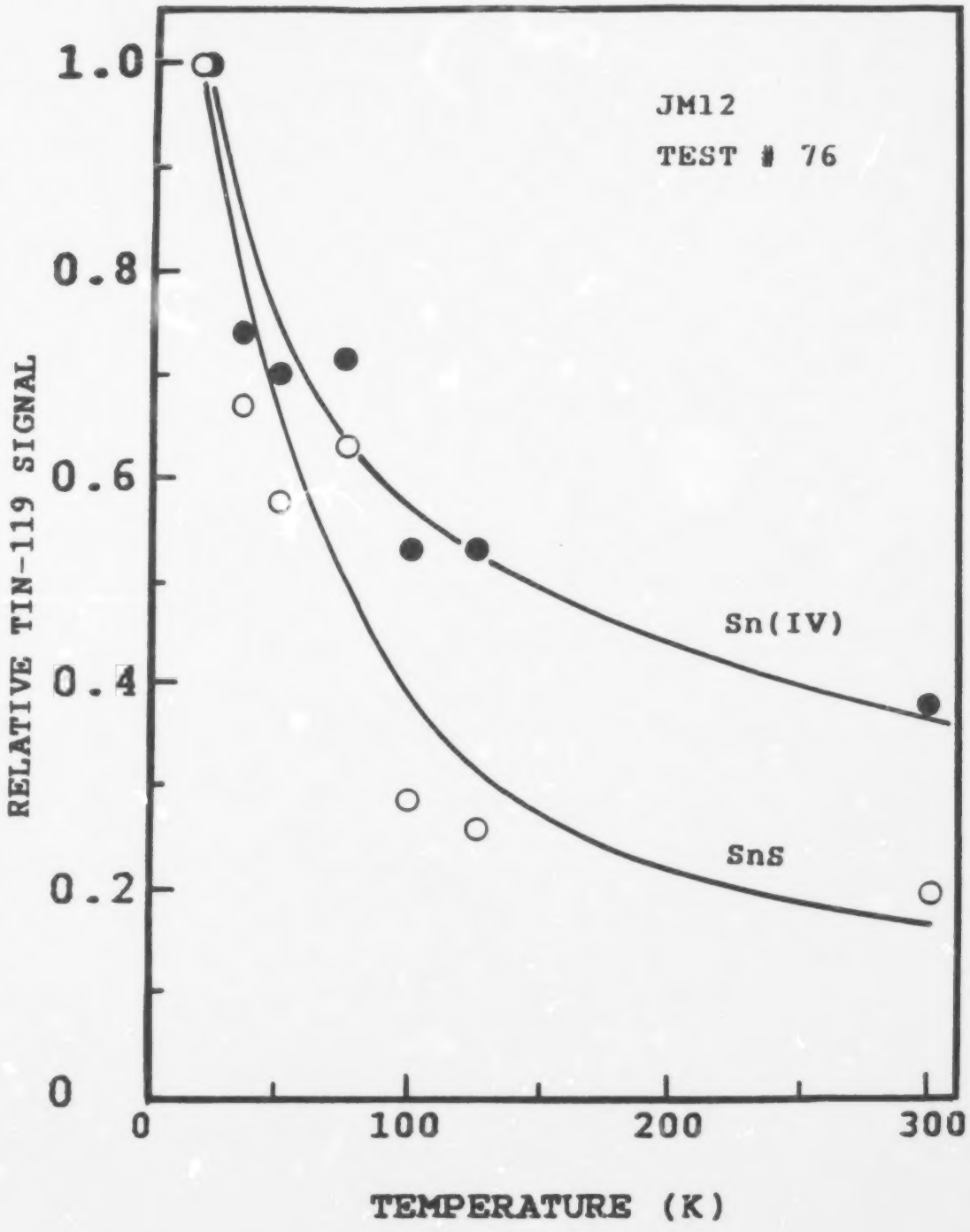

Figure 27: Relative tin-119 Mössbauer signal versus temperature for JM12 used catalyst.

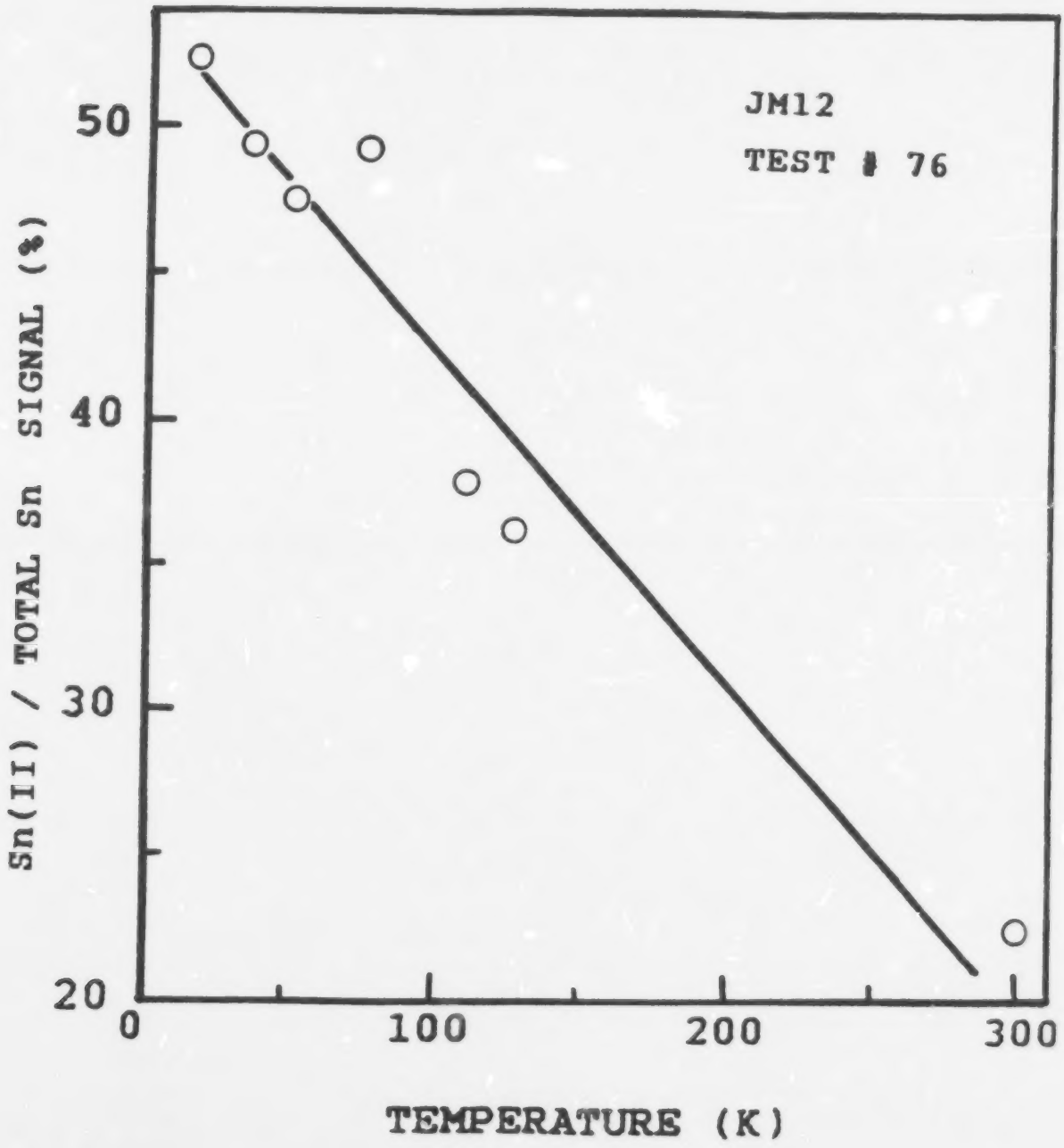

Figure 28: Ratio SnS/Total tin Mössbauer signal versus temperature for JM12 used catalyst.

found that the recoil-free fractions of SnS and Sn(IV) to be similar. We have no explanation for this anomalous behavior. Combining the results for tin(IV) oxide and for SnS in the used catalysts, we find that the tin(IV) oxide is reduced to about 67 % in going from 15 K to RT, whereas the SnS signal drops to 22 % of its low temperature value. Therefore, the intensity of the SnS signal at RT should be multiplied by a factor of ca. 3 in order to obtain meaningful quantitative evaluation of the relative amounts of tin(IV) oxide and SnS in the used catalysts. Table X compares estimated values of the relative amount of the two tin-containing components in the used catalysts, after correction for the difference in recoil-free fractions using our variable temperature Mössbauer spectroscopic results. Obviously, the smallest corrections are required for signals close to 0 % and to 100 % (fig. 29).

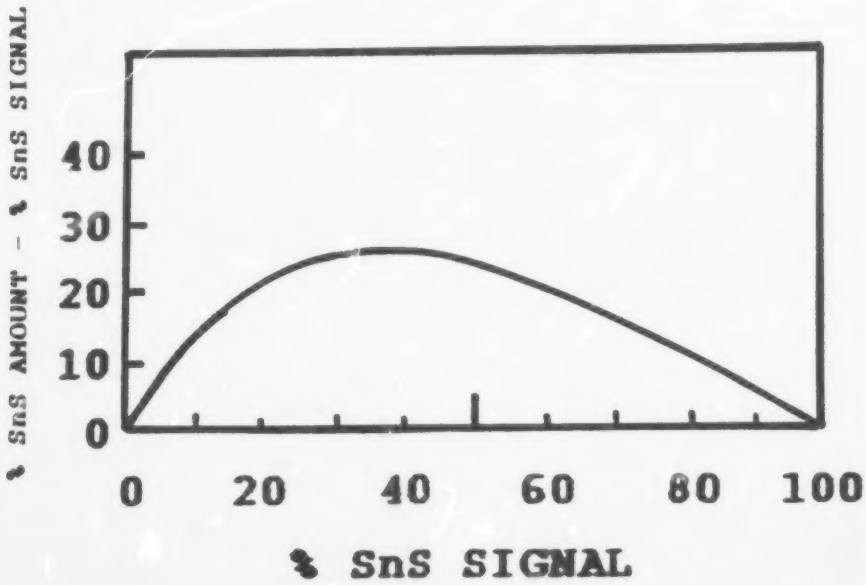

Figure 29: Difference between the % amount of SnS and its % Mössbauer signal in the used catalysts.

Table I: Estimation of the relative amounts of tin(IV) oxide and SnS in the used catalysts after correction for difference in recoil-free fractions using variable temperature Mössbauer spectroscopy.

Sample	Catalyst	Species	% signal at RT	% amount	Difference
JM4	MB-586	Sn(IV)	99	97	2
		SnS	1	3	2
JM6	MB-587	Sn(IV)	>99	~99	-
JM11	MB-599	Sn(IV)	85	65	20
		SnS	15	35	20
JM12	MB-599	Sn(IV)	90	75	15
		SnS	10	25	15
JM20	MB-590	Sn(IV)	27	11	16
		SnS	73	89	16
JM21	MB-590	Sn(IV)	22	9	13
		SnS	78	91	13
JM22	MB-599	Sn(IV)	82	60	22
		SnS	18	40	22
JM26	MB-590	Sn(IV)	34	15	19
		SnS	66	85	19
JM27	MB-590	Sn(IV)	24	10	14
		SnS	76	90	14
JM28	MB-599	Sn(IV)	85	65	20
		SnS	15	35	20
JM31	MB-590	Sn(IV)	30	13	17
		SnS	70	87	17

CONCLUSION

The solid state techniques present in our laboratory have proved very useful for the characterization and an in-depth study of supported catalysts prepared in the Energy Research Laboratories of CANMET. The techniques we used are X-ray powder diffraction, scanning electron microscopy and Mössbauer spectroscopy. The latter was performed as a function of temperature, in the range 15-300 K, with the help of a closed cycle helium refrigeration system. Tin-119 was used to probe the active metal site in tin-containing catalysts.

The catalysts were investigated at various stages of preparation and use. Typically, three stages were studied: (i) after ionic exchange, (ii) after calcination, and (iii) after use and separation from hydrocarbons. In addition, the supports and intermediate products formed in the preparation of the supports were also examined. Moreover, some used catalysts were also studied at two intermediate stages before separating heavy hydrocarbons, i.e. (i) before homogeneizing the mixture of heavy hydrocarbons and solid residue, and (ii) after homogeneizing. Two kinds of supports were used in the preparation of the catalysts at CANMET, one was coal, and all the others were hydrous titanate. For most of the samples we received for investigation, tin was the active metal. However, we were also provided with a sample, calcined at three different temperatures, with cobalt and molybdenum as active metals.

All samples are characterized by their small particle size. This is evidenced by the absence of a powder pattern when the samples are completely amorphous, or by broadened Bragg peaks in less severe cases of microcrystallinity. These results are corroborated by the general lack of texture and of particle shape observed in electron microscopy. The catalysts appear as very

fine powders, often lumped together in loose agglomerates, which have no defined shape. Sintering does not occur upon calcination or testing. The supports and intermediate products, as well as the tin chloride supported on coal are completely amorphous to X-rays. The tin catalysts supported on hydrous titanates usually show a very weak evidence of microcrystallinity for SnO_2 and TiO_2 with an average particle diameter much lower than 100 Å. Limited recrystallization takes place on calcining at 400 °C, however, the crystalline phases obtained are still microcrystalline. These are usually a mixture of TiO_2 anatase (~300 Å), SnO_2 and TiO_2 rutile (~100 Å), or a $Ti_{1-x}Sn_xO_2$ solid solution. This solid solution partly decomposes during hydroprocessing and liberates TiO_2 anatase and "activated" SnO_2 which is reduced by H_2 and C to Sn(II) and sulfided to SnS. The cobalt/molybdenum catalysts supported on hydrous titanate is amorphous up to at least 350 °C. After calcination at 500 °C, it yields TiO_2 anatase, $CoMoO_4$, and maybe $Co_2Mo_3O_8$, CoO and Co_3O_4.

The thermal behavior of the hydrous titanate support was often found not to be dependent on the nature of the metal deposited on it. For example, both with Sn and Co-Mo, TiO_2 anatase was formed upon calcination. This is not surprising since anatase is the stable form of TiO_2. However, there are some exceptions. In some cases, the deposited metal influenced the crystallization of the support on calcining: with Sn, SnO_2 rutile (stable form of SnO_2) induced the formation of TiO_2 in the rutile form (normally unfavored form) and of rutile type $Ti_{1-x}Sn_xO_2$ solid solution. In another experiment, JM14 sodium hydrous titanate, not loaded with another metal, was calcined in the same conditions than the catalysts, however, X-ray diffraction showed that no Bragg peaks were present, and therefore no crystalline material had formed. This is probably due to the presence of sodium in the hydrous titanate support.

The formation of SnS is mostly a function of the ease of cleavage of the Sn(IV) bonds to its surrounding, i.e. to the ability of tin(IV) to be first reduced to tin(II), which, then, can be sulfided to SnS. The formation of SnS was never observed from SnO_2; this is probably due the high strength of the lattice of tin(IV) oxide. Depending on the nature of the tin present in the catalyst, t.. following is observed:

- SnO_2: very stable, highly unreactive ===> no SnS;
- $Ti_{1-x}Sn_xO_2$ solid solution: less stable ===>partly decomposed;
- JM5 (Sn-Cl bonds): more labile ===> completely decomposed.

Mössbauer spectra taken on the same used catalysts before and after homogeneizing the mixture of heavy hydrocarbons and solid residue shows that little if any decrease of the amount of SnS is observed after homogeneization. This is not surprising since the heavy hydrocarbons prevent air from reaching the used catalyst immersed in it.

Variable temperature Mössbauer spectroscopy was very useful for an adequate determination of the relative amounts of tin(II) and tin(IV) in the catalysts. Because the recoil-free fraction of soft lattice compounds decreases drastically with increasing temperature, ambient temperature studies only yield highly underrated estimations for these materials, primarily tin(II) compounds (SnS) and tin(IV) chloride supported on coal, in the case of the catalysts investigated. In contrast, tin(IV) oxides have a very hard lattice, therefore their recoil-free fraction decreases very slowly as temperature is raised, and as result, they are highly overestimated from ambient temperature spectra. The evolution of the relative intensity of the subspectrum for each kind of tin with temperature makes it possible to correct for most of their difference in recoil-free fraction. In order to give a more striking evidence of the importance of the recoil-free fraction problem, the results for all variable temperature experiments shown on fig. 10-11 and 22-28 are grouped on fig. 30,

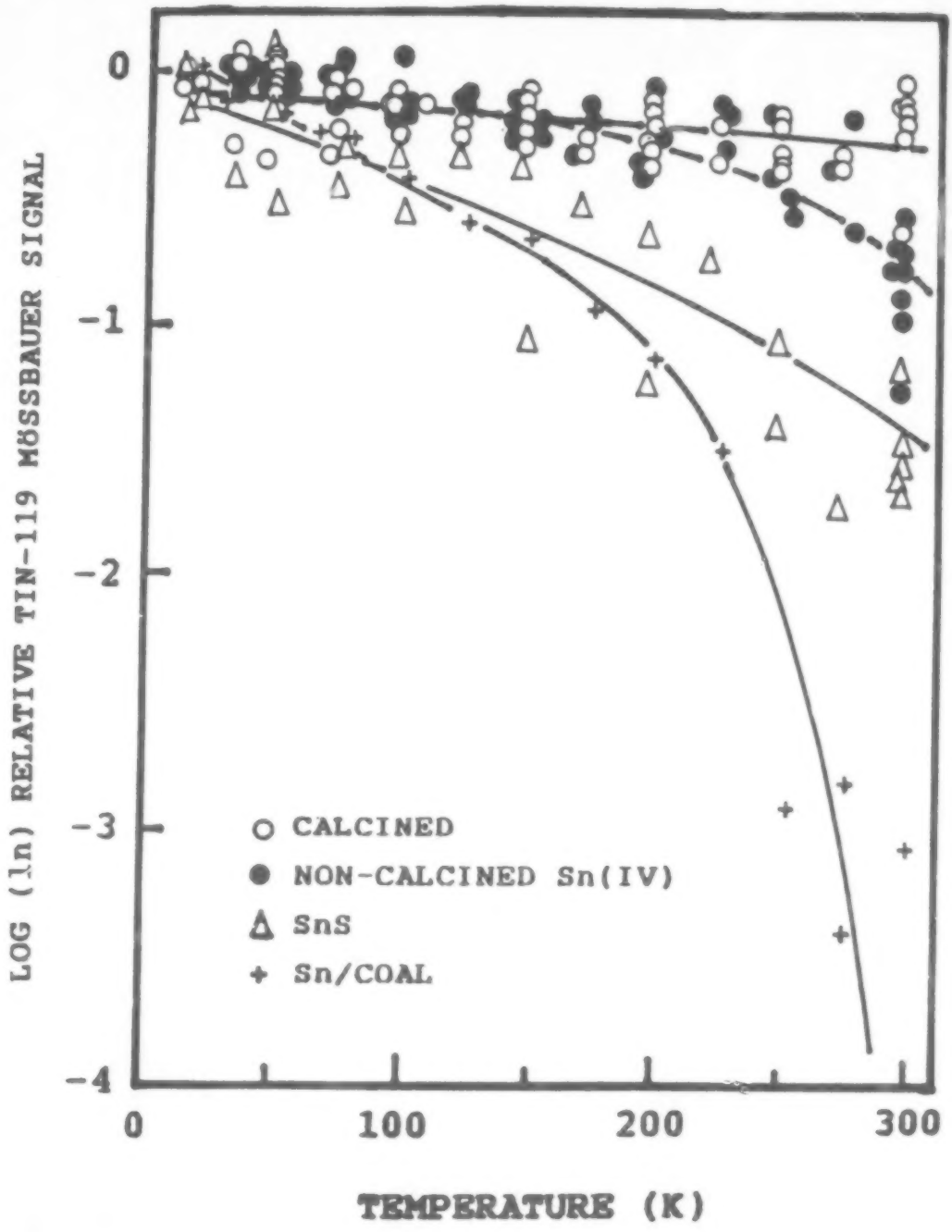

Figure 30: Comparison of the lattice strength of the stable tin species encountered in tin catalysts supported on hydrous titanate or on coal, as probed by the change of recoil-free fraction versus temperature in tin-119 Mössbauer spectroscopy.

all at the same scale. The tin(IV) oxides found in the calcined catalysts have the highest recoil-free fraction as expected. The recoil-free fraction for the tin(IV) oxides present in non-calcined catalysts is the same than after calcination up to ca. 150 K. However, above that temperature, their recoil-free fraction decreases slightly, but significantly faster. This can be attributed to the hydration of these phases. Most likely, some of the Sn-O bonds in the non-calcined catalysts involve $Sn-OH_2$ and perhaps Sn-OH, whereas, in SnO_2, every oxygen atom is coordinated to three tin atoms, as follows:

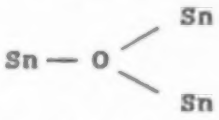

and each tin is octahedrally (slightly distorted) coordinated to six oxygen atoms. It results that the lattice of SnO_2 is very strong, whereas the presence of non-bridging H_2O molecule and/or OH^- anions softens the lattice locally at tin. In addition, the smaller particle size of the non-calcined catalysts (evidenced by X-ray diffraction) may contribute to lowering the recoil-free fraction.

The recoil-free fraction of SnS is much more sensitive to an increase in temperature. This is expected, as a general feature of tin(II) compounds, due to a lower dimensionality in bonding, at least locally, and quite often over the whole lattice. Interruption in bonding in some directions is due to the stereo-active non-bonding electron pair so characteristics of divalent tin, and more generally, of suboxidation states in main group elements. The case of $SnCl_2.2H_2O$ impregnated on coal is even more striking. Mössbauer spectroscopy shows that all tin is oxidized to tin(IV), perhaps by oxygen present at the surface on the coal particles, and it is coordinated by a mixture of chlorine and oxygen ligands. In addition, the spectrum at RT is so weak as almost escaping detection. However, a very strong

spectrum is obtained at low temperatures. This is probably due to the weaker nature of the Sn-Cl bonds and, most likely, to the fact that the amorphous tin(IV) oxichloride (the X-ray powder pattern has no Bragg peak) is present in the form of a thin layer on the surface of the coal particles.

A surprising feature of the non-calcined catalysts was the low amount of divalent tin. This was attributed to the nature of the solutions used for their preparation (pH, dissolved oxygen). However, this could not fully explain how tin(II) got oxidized to tin(IV). Low temperature Mössbauer spectroscopy, carried out to take into account the difference in recoil-free fraction, showed all tin(II) had disappeared between the RT and low temperatures measurements. This shows air oxidized divalent tin slowly in the catalysts, and suggests that it was present as a highly divided material.

RECOMMENDATIONS

The choice of the solid state techniques for the study of the catalysts is highly praised. They have provided a wealth of information usually not attainable by other means. In other cases, they have also corroborated or complemented information previously obtained. The main interest in the choice of techniques is their suitability for studying the catalysts, and their remarkable complementarity. Indeed, electron microscopy shows the texture of the material and particle shape and size for "large" particles (micrometer range). On the other hand, X-ray diffraction cover the range ca. 30-1,000 Å. In addition, X-ray diffraction allows a unambiguous identification of all crystalline phases by probing the whole crystal lattice of each phase, however, it cannot detect non-crystalline phases. Mössbauer spectroscopy allows identification of all tin phases present, regarless of their degree of crystallinity, however, it is restricted to tin, since tin-119 was the probe used. In addition, variable temperature Mössbauer spectroscopy provides a very elegant way of probing the lattice strength of the tin-containing phases, and thereby makes possible quantitative evaluations of each tin-containing phase in a mixture. We have shown above that ambient temperature spectra only provide highly inaccurate quantitative estimations.

We recommend the following:

1. The use of the same techniques in combination for future studies of related samples;

2. The preparation of tin(II) catalysts in deoxygenated solutions, and the handling and storage of these catalysts in oxygen-free atmosphere. This would allow the stabilization of these materials for adequate characterization and tests.

REFERENCES

1. J. Monnier and J. F. Kriz, ACS Preprints, Div. of Petroleum Chemistry 30, 513 (1985).

2. J. Monnier and J.F. Kriz, 10th Canadian Symposium on Catalysis, Preprints, 1-8 (1986).

3. J. Monnier, G. Denes, J. Potter and J.F. Kriz, Energy & Fuels 1, 332-338 (1987).

4. J. Monnier, C. W. Fairbridge, J. R. Brown and J. F. Kriz, Proc. 9th Int. Congress Cat., eds. M. J. Phillips & M. Ternan, Vol. 1, 182-189 (1988).

5. R.G. Dosch, H.P. Stephens and F.V. Stohl, U.S. Patent 4,511,455 (1985).

6. H.P. Stephens, R.G. Dosch and F.V. Stohl, Ind, Eng. Chem. Prod. Res. Dev. 24, 15 (1985).

7. H.P. Stephens and R.G. Dosch, Proc. 9th Int. Congress Cat., eds. M. J. Phillips & M. Ternan, Vol. 1, 160-165 (1988).

8. F. A. Cotton and G. Wilkinson, "Advanced Inorganic Chemistry", Wiley, New-York, 5th edit., 655 (1988).

9. G. Denes, "Characterization of Tin catalysts by Mössbauer Spectroscopy", Final report to CANMET, under Supply and Services, Contract serial number 0ST85-00243, Department of Chemistry and Laboratories for Inorganic Materials, Concordia University, Montreal, Quebec, Canada (1987).

10. G. Denes and J. Monnier, ACS Preprints, Div. of Fuel Chemistry 33, 403-414 (1988).

11. G. Denes and J. Monnier, "Production and Processing of Fine Particles", ed. A. J. Plumpton, Can. Inst. Mining and Met., Pergamon, New York, 637-647 (1988).

12. N. N. Greenwood and T. C. Gibb, "Mössbauer Spectroscopy", Chapman and Hall, London (1971).

13. T. C. Gibb, "Principles of Mössbauer Spectroscopy", series "Studies in Chemical Physics", Chapman and Hall, London (1976).

14. J. Galy, G. Meunier, S. Anderson and A. Aström, J. Solid State Chem, 13, 142-159 (1975).

15. I.D. Brown, J. Solid State Chem. **11**, 214-233 (1974).

16. J. Pannetier and G. Denes, Acta Cryst. B**36**, 2763-2765 (1980).

17. G. Denes, J. Solid State Chem. **74**, 343-352 (1988).

18. J. Pannetier, G. Denes, M. Durand and J. L. Buevoz, J. Physique **41**, 1019-1024 (1980).

19. G. Denes, J. Pannetier and J. Lucas, J. Solid State Chem. **33**, 1-11 (1980).

20. G. Denes, J. Pannetier, J. Lucas and J. Y. Le Marouille, J. Solid State Chem. **30**, 335-343 (1979).

21. T. Birchall, G. Denes, K. Ruebenbauer and J. Pannetier, Hyperf. Inter. **29**, 1331-1334 (1986).

22. V. A. Bryukhanov, N. N. Delyagin, A. A. Opalenko and V. S. Shpinel, Soviet Physics JETP Engl. Transl. **16**, 310 (1963), [J. Exptl. Theoret. Phys.(U.S.S.R.) **44**, 393 (1963)].

23. T. Birchall, G. Denes, K. Ruebenbauer and J. Pannetier, J. Chem. Soc. Dalton Tr., 2296 (1981).

24. G. Denes, J. Solid State Chem. **77**, 54-59 (1988).

25. C. Kittel, "Introduction to Solid State Physics", 5th Edition, John Wiley & Sons, New York (1976), chapters 4 & 5.

26. R. Herber and S. Chandra, J. Chem. Phys. **52**, 6045 (1970).

27. T. Birchall, G. Denes, K. Ruebenbauer and J. Pannetier, Hyperf. Inter. **29**, 1327-1330 (1986).

28. T. Birchall, G. Denes, K. Ruebenbauer and J. Pannetier, Hyperf. Inter. **30**, 167-183 (1986).

29. A. J. F. Boyle and H. E. Hall, Repts. Progr. in Physics **25**, 441 (1962).

30. J. S. Van Wieringen, Phys. Letters **26A**, 370-371 (1968).

31. P.Z. Hien and V.S. Shpinel, Soviet Physics JETP Engl. Transl. **17**, 268 (1963), [J. Exptl. Theoret. Phys.(U.S.S.R.) **44**, 393 (1963)].

32. "Powder Diffraction File - Inorganic Phases", JCPDS, International Centre for Diffraction Data, Swarthmore, PA (1988). [JCPDS= Joint Committee on Powder Diffraction Standards. The "Powder Diffraction File" is often called the "JCPDS File", and was formerly known as the "ASTM File"].

33. B. D. Cullity, "Elements of X-ray Diffraction", 2nd edition, Addison-Wesley Publishing Co, Inc., Don Mills, Ontario, pages 192 & 284 (1978).

34. A. R. West, Solid State Chemistry and its Applications", John Wiley & Sons, New-York (1984).

35. E. M. Baggio and T. J. Sonnino, J. Chem. Phys. 52, 3786 (1970).

36. P.S. Cook, J.D. Cashion and P.S. Cassidy, Fuel 64, 1121 (1985).